Title

Single-cell transcriptomic analysis of macaque LGN neurons reveals novel subpopulations

Authors

Shi Hai Sun[1,2*], Kai Renshaw[1,3,*], John S. Pezaris[1,2]

* Equal Contribution

Correspondence: John S. Pezaris; Pezaris.John@mgh.harvard.edu

Affiliations

[1]Department of Neurosurgery, Massachusetts General Hospital, Boston, Mass., USA

[2]Department of Neurosurgery, Harvard Medical School, Boston, Mass., USA

[3]Tufts University School of Medicine, Boston, Mass., USA

Conflicts of Interest

The authors declare no competing interests.

Funding

Supported by Peter and Yayi Pezaris, Don Good, Michael Gersh, NIMA Foundation, NIH EY027888, and the William M. Wood Foundation, Bank of America, Trustee.

Abstract

Neurons in the lateral geniculate nucleus (LGN) provide a pivotal role in the visual system by modulating and relaying signals from the retina to the visual cortex. Although the primate LGN, with its distinct divisions (magnocellular, M; parvocellular, P; and koniocellular, K), has been extensively characterized, the intrinsic heterogeneity of LGN neurons has remained unexplained. With the development of high-throughput single-cell transcriptomics, researchers can rapidly isolate and profile large sets of neuronal nuclei, revealing a surprising diversity of genetic expression within the nervous systems, such as two types of K neurons (Bakken *et al.*, 2021). Here, we analyzed the transcriptomes of individual cells belonging to macaque LGN using raw data from a public database to explore the heterogeneity of LGN neurons. Using statistical analyses, we found additional subpopulations within the LGN transcriptomic population, whose gene expressions imply functional differences. Our results suggest the existence of a more nuanced complexity in LGN processing beyond the classic view of the three cell types and highlight a need to combine transcriptomic and functional assessments. A complete account of the cell type diversity of the primate LGN is critical to understanding how vision works.

36 # Introduction

37 The lateral geniculate nucleus (LGN) of the thalamus serves as the main relay through which
38 visual information travels from the retina to the cortex (Sherman & Guillery, 2006; Solomon &
39 Lennie, 2007). Within LGN, visual input is segregated both spatially – distinct areas of the visual
40 field correspond to distinct areas of LGN (Chen et al., 1999; K. A. Schneider et al., 2004) – and
41 functionally (Denison et al., 2014; K. A. Schneider et al., 2004). A bulk of research has focused
42 on determining the precise spatial, functional, and morphological organization of LGN, as a
43 better understanding of LGN's organization can provide insight into visual processing and has
44 important clinical relevance.

45 In primates, LGN is composed of distinct layers of functionally similar cell types:
46 magnocellular (M), parvocellular (P), and koniocellular (K). Electrophysiological and
47 morphological studies in primates have determined the specific characteristics of these layers: M
48 neurons, which are large in size and receive rod photoreceptor-derived information, are well-
49 suited for rapid temporal dynamics and detecting motion; P neurons, receiving cone
50 photoreceptor-derived information, are attuned to chromatic changes, making them optimal for
51 processing color and form; and less well-defined K neurons receive short-wavelength ("blue")
52 photoreceptor-derived information (Hubel & Livingstone, 1990; Maunsell et al., 1999; Reid &
53 Shapley, 2002; Tailby et al., 2008; Wiesel & Hubel, 1966).

54 As methods for electrophysiological investigation improve, evidence has been
55 accumulating for functional heterogeneity within the three primary LGN cell types. For instance,
56 *on*- and *off*-specific responses from the retina are preserved within distinct populations of M, P,
57 and K cells (Ichinose & Habib, 2022; Rousso et al., 2016). K cells have also been shown to

58 express receptive fields with non-standard features, including orientation sensitivity, contrast
59 suppression, and many others (Cheong et al., 2013; Eiber et al., 2018; Solomon et al., 2010).
60 Lastly, a recent electrophysiological analysis identified visually responsive LGN cells that did
61 not exhibit any M, P, or K functional responses, suggesting a functional complexity beyond the
62 M, P, and K classification (Sun et al., 2024). All this evidence points toward the existence of
63 multiple subpopulations of LGN neurons within M, P, and K cell types.

64 Most recently, single-cell RNA-sequencing technologies have been developed for
65 transcriptomic profiling, enabling the identification of cellular subclasses of cells by comparing
66 the gene expression patterns across large numbers of individual cells within a tissue sample (Lein
67 et al., 2017; Lowe et al., 2017; Ståhl et al., 2016). While past attempts to understand the
68 organization of LGN have relied primarily on morphology and electrophysiology, we
69 hypothesize transcriptomic analysis of LGN neurons will reveal more details about their
70 organization and functional roles in visual processing. For example, single-cell RNA-seq studies
71 in macaque have identified 13 transcriptomically separable excitatory cell classes in V1 (Wei et
72 al., 2022) and more than 60 distinct cell types in the retina (Peng et al., 2019), while only four
73 excitatory cell types were reported in the LGN (Bakken et al., 2021). In the present study, we
74 explore the transcriptomic diversity of macaque LGN neurons using raw data obtained from a
75 published database (Bakken et al., 2021). Statistical analyses of the LGN transcriptomes revealed
76 seven subpopulations of excitatory LGN neurons: two magnocellular populations, two
77 parvocellular populations, and three koniocellular populations. We show that these
78 subpopulations differentially express gene profiles, which imply specific functional differences
79 between these putative subclasses. Our results suggest that there is further nuance in the
80 functional organization of LGN that may be reflected in its role in visual processing.

Methods

RNA data

The RNA-seq data consisting of 2,157 macaque nuclei and accompanying metadata were sourced from the Allen Brain Map (Allen Institute for Brain Science, 2022), available at https://portal.brain-map.org/atlases-and-data/rnaseq/comparative-lgn, and originally used in (Bakken *et al.*, 2021). For single-cell/-nucleus processing for RNA sequencing and processing, please see Tasic *et al.* (2018); Bakken *et al.* (2018, 2021); Hodge *et al.* (2019) for the complete details. In summary, nuclei were isolated by Fluorescence-Activated Cell Sorting, enriched for neurons with neuronal markers, processed with SMART-seq v4 (Clontech) and Nextera XT (Illumina), and sequenced on HiSeq 2500 (Illumina). RNA-seq reads were aligned to corresponding genomes using the STAR aligner (Dobin et al., 2013), and samples had a median depth of 1.3 million reads/nucleus.

Preprocessing

Data preprocessing and analyses were performed in R using Seurat v5 (Butler et al., 2018; Hao et al., 2024; Stuart et al., 2019) as Seurat consistently outperforms other modern algorithms (Fu et al., 2025). We used a customized version of the standardized single-cell transcriptomics analysis workflow (Clarke et al., 2021), as described below.

Using the supplied metadata from the (Allen Institute for Brain Science (2022) and Bakken *et al.* (2021), low-quality cells (cells that did not pass quality control criteria: <100,000 total reads, <1,000 detected genes, < 75% of reads aligned to genome, or CG dinucleotide odds

ratio > 0.5; Tasic *et al.*, 2018) and genes (e.g., uncharacterized or non-informative genes) were removed from all further analyses. All cells were prelabeled as M, P, K (Kap and Kp), GABA (GABA 1-4), or pulvinar, as defined in the metadata. Since this study is a comparison of LGN M, P, and K excitatory cells, GABA and pulvinar cells were removed from further analyses (61% remaining, n = 1,309 / 2,157).

Clustering

M, P, and K cell sets were processed separately using cluster analysis to explore the heterogeneity of LGN neurons. Before clustering, the data was preprocessed and normalized using the Seurat function *SCTransform*, which uses a regularized negative binomial regression model for normalization and analytic Pearson residuals to find top variable genes for downstream analysis (Choudhary & Satija, 2022; Lause et al., 2021). For batch correction, we used *IntegrateLayers* with *HarmonyIntegration*, which integrates cells from multiple datasets (Korsunsky *et al.*, 2019). The processed data was then dimensionally reduced using principal component analysis (PCA, via *RunPCA*). Clustering was performed using *FindNeighbors,* K-nearest neighbor (KNN), and *FindClusters*, which uses the Louvain algorithm for cluster identification. The clustering results were visualized using uniform manifold approximation and projection (UMAP, via *RunUMAP*; McInnes *et al.*, 2020), and quantitatively evaluated using silhouette scores to assess cluster separation.

To find the optimum parameters to use for the analysis, a global parameter optimization strategy using silhouette scores as the objective metric was used. Specifically, for each of the M, P, and K cell subsets, the optimum number of principal components (PCs), number of features

124 (highly variable genes in *SCTransform*), and clustering resolution (*FindClusters*) were
125 determined.

126 First, to obtain the optimal number of PCs, the standard deviation of each PC was plotted
127 across a range of feature counts (1,000 to 4,000 in increments of 500) using Seurat's *ElbowPlot*
128 function. The point where the curve plateaued was selected qualitatively as the optimal number
129 of PCs for each of the M, P, and K cell types. Because the location of the elbow is subjective, we
130 followed the recommendation of the Seurat developers to favor the higher side when choosing
131 this parameter.

132 Next, a global parameter search was conducted to identify the combination of feature
133 number and clustering resolution that maximized the average silhouette width. The number of
134 features ranged from 1,000 to 4,000 in steps of 100 and the clustering resolution values spanned
135 from 0.1 to 1.0 in increments of 0.02. For each combination, clustering was performed following
136 dimensionality reduction by PCA, using the optimum number of PCs as defined above, and
137 silhouette scores were computed. A Generalized Additive Model (GAM) was then fitted to
138 smooth the silhouette score surface and remove outliers. The parameters corresponding to the
139 peak predicted silhouette score were selected for each cell type group. The final clustering
140 parameters for M, P, and K cell types are specified in the Results section. See Figure 1B for a
141 visualized map of the described clustering workflow.

142 Clustering validation testing

143 To assess robustness, a sensitivity analysis was performed. This included random downsampling
144 of each dataset to 70-90% of the original cells, as well as ±20% variation in the number of highly
145 variable genes and ±1 variation in the number of dimensions used for clustering. This process

146 was bootstrapped and repeated 1,000 times, and the findings are referenced in the Results and
147 Discussion sections.

148 To assess the clustering stability we added Gaussian noise directly to the Harmony
149 embeddings, scaled to 20% of the standard deviation (SD) of each embedding dimension. For
150 each cluster group, we performed 1000 iterations of added noise while preserving the original
151 cluster labels, and computed the silhouette score for each perturbed embedding. An empirical *p*-
152 value was calculated as the proportion of noise-affected silhouette scores that were equal to or
153 greater than the silhouette score from the original data. Cluster degradation was defined as the
154 percentage decrease in silhouette relative to the original value.

155 As an external validation of the clustering approach, an in-silico benchmark was
156 conducted using a publicly available, cell-sorted peripheral blood mononuclear cell (PBMC)
157 single-cell RNA-seq dataset with established ground-truth labels from Wang *et al.* (2019),
158 downsampled from Zheng *et al.* (2017). The dataset was first clustered using the standard Seurat
159 workflow, consistent with methods used in Bakken *et al.* (2021), to broadly identify the immune
160 cell populations. Subsequently, the heterogeneous cluster from the initial analysis was re-
161 clustered using the optimized silhouette-based global parameter search pipeline, as described
162 above. To evaluate stability, the analysis was also repeated under downsampling conditions and
163 across multiple bootstrap iterations. The details and results of this validation experiment are
164 presented in Supplementary Figure 1 and referenced in the Results.

165

166 **Differentially expressed genes**

167 Each cluster was profiled through differential gene expression for comparative analysis.
168 Differentially expressed genes/markers (we will use *genes* and *markers* interchangeably) were
169 determined with the Seurat function *FindAllMarkers*, defined with an adjusted *p*-value < 0.05
170 (Wilcoxon Rank Sum test). We also defined these genes as biologically significant if the $\log_2$
171 fold change is greater than 1 (i.e., log2FC > 1 and adjusted *p*-value < 0.05). Gene expression
172 profiles were visualized using heat maps (*DoHeatMap*) and dot plots (*DotPlot*). For the gene
173 ontology analysis, ToppGene (https://toppgene.cchmc.org/enrichment.jsp) and the National
174 Center for Biotechnology Information (NCBI) Gene database
175 (https://www.ncbi.nlm.nih.gov/gene/) were used. As the interpretation of gene ontology results is
176 necessarily speculative, most of this analysis is presented in the Discussion section.

177 **Results**

178 We analyzed the transcriptomes of 1,309 nuclei from microdissected, anatomically defined
179 regions of the macaque lateral geniculate nucleus (LGN) using RNA-seq data sources from the
180 Allen Brain Map (Allen Institute for Brain Science, 2022; Bakken et al., 2021). The RNA-seq
181 data was preprocessed by removing low-quality cells and unnecessary genes (see Methods), as
182 per the metadata provided by the Allen Institute (Allen Institute for Brain Science, 2022). Like in
183 Bakken *et al.* (2021), the gene expression was quantified as the sum of intron and exon reads,
184 normalized as counts per million (CPM), and $\log_2$-transformed. Each cell was categorized into
185 one of the predefined clusters (M, P, K) based on the metadata associated with the published data
186 set (Bakken et al., 2021). These cells in their predefined labels are shown in Figure 1A,

illustrating the cell-to-cell genetic diversity in a dimensionally reduced UMAP (Uniform Manifold Approximation and Projection) plot.

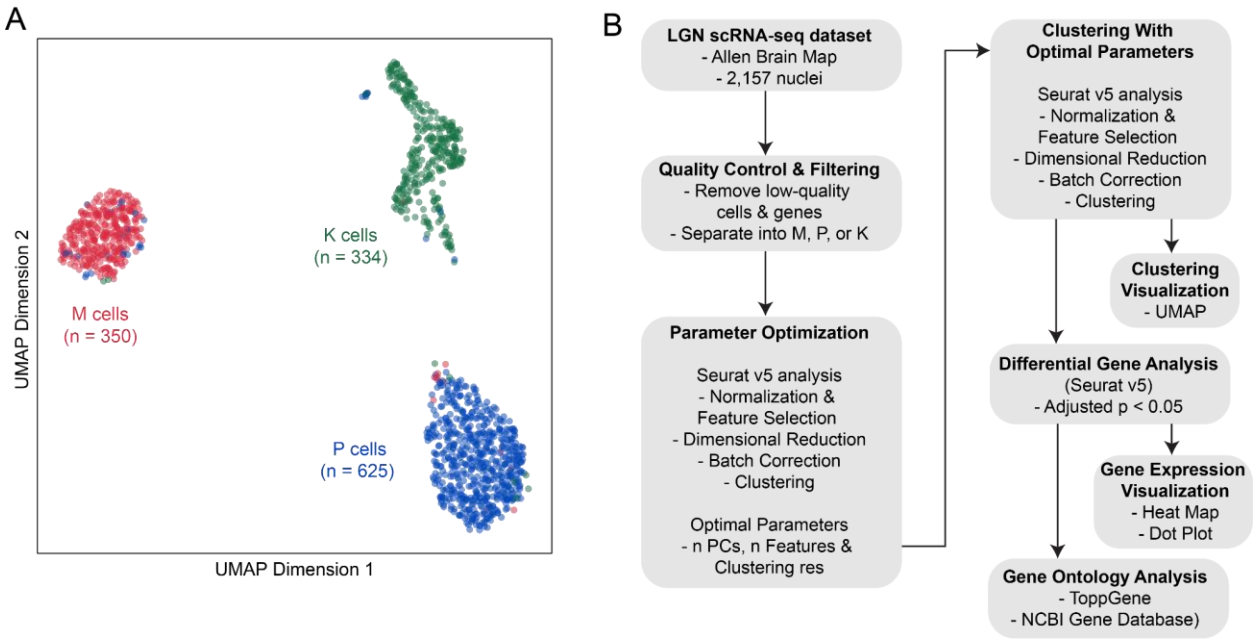

Figure 1. Analysis pipeline of LGN scRNA-seq data, sourced from the Allen Brain Map. **(A)** Scatter plot visualization for each cell (n = 1309) in UMAP space, where the horizontal and vertical axes represent the dimensionality-reduction UMAP coefficients. The magnocellular (M), parvocellular (P), and koniocellular (K) cells are illustrated as red, blue, and green, respectively. **(B)** Flow chart of the clustering and gene analysis. As labeled in the supplied metadata, sets of the M, P, and K cells were individually preprocessed. Each group of cells went through parameter optimization and then clustered using Seurat v5. Differential genes were collected and annotated with each cell population.

Given the wide diversity within primate retinal ganglion cells (Dacey, 2004; Peng et al., 2019), our increasing understanding of the complexity of the LGN (Sun et al., 2024) and the

visual cortex (Vries et al., 2020; Wei et al., 2022), we believe cellular subtypes within M, P, and K are to be discovered and expect they can be distinguished using transcriptomics. Therefore, each of the M (n = 350), P (n = 625), and K cell (n = 334) groups from the publicly sourced dataset were reanalyzed using an adjusted Seurat analysis pipeline (Figure 1B). Notably, because there are no universally accepted standards for the function parameter selection in the Seurat analysis pipeline (Arbatsky et al., 2025) and the default parameters are inherently arbitrary (I. Schneider et al., 2021), we employed a global optimization approach to optimize for cluster separation quality (Silhouette score) to determine the optimum number of principal components (PCs), number of features, and clustering resolution for each cell type (see Methods).

To confirm the robustness of the clustering pipeline, we first validated the workflow using a ground-truth-labeled PBMC single-cell RNA-seq dataset. The clustering achieved a 90.7% accuracy match to the known labels, with a moderate silhouette score of 0.276 (Supplementary Figure 1). Stability testing through 100 iterations of downsampling and varying the number of features and dimensions yielded a mean cluster identity match of 89.63% (SD = 1.23%), confirming that the pipeline reliably recovers biologically meaningful subpopulations

Our M, P, and K clustering results using the adjusted Seurat analysis pipeline will be described below in threefold: (1) how many within-cluster subpopulations (i.e., clusters within M, P, or K sets) are evident in the data along with the optimized parameters used; (2) what are the significant genetic differences that define these subpopulations; and (3) what functions and interpretations can we infer using genetic annotation from public resources. Much of the interpretation from (3) will be in the Discussion section. Throughout the Results and Discussion, we define significant genes as those with an adjusted p-value < 0.05, and biologically significant genes as those with both an adjusted p-value < 0.05 and a fold-change > 2 (or log2FC > 1).

224 However, because the definition of biological significance is somewhat arbitrary (Dalman et al.,
225 2012), and informative genes can exhibit moderate fold changes of less than 2 (St. Laurent et al.,
226 2013), we will consider both significant and biologically significant genes, while explicitly
227 noting fold-change values throughout.

228

229 **M cell clustering**

230 Two subpopulations emerged from the set of M cells: M_1 (n = 226) and M_2 (n = 124).
231 The optimized parameters used were 4 PCs, 2800 top features, and a cluster resolution of 0.2
232 (Figure 2A). After GAM fitting (for smoothing and outlier removal), these parameters produced
233 a silhouette score of 0.231, indicating a low to moderate within-cluster cohesion and inter-cluster
234 separation between M_1 and M_2 cells. The two clusters using the optimized parameters can be
235 visualized in the UMAP plot of Figure 2B. Likewise, when only considering the significant
236 genes from these populations (n genes = 185), the UMAP plot in Figure 2C illustrates an ideal
237 separation between the two subpopulations with a silhouette score of 0.36, though we
238 acknowledge this is somewhat circular since gene selection was based on differential expression.

239 We also performed stability and sensitivity analyses to assess the robustness of the
240 clustering. Downsampling the number of cells (70-90%), varying the number of highly variable
241 genes (80-120%) and number of PCs (±1), consistently reproduced two M clusters in 71.5% of
242 bootstrap iterations (n = 1000), with an average cluster identity match of 86.0 ± 6.0%. This
243 indicates that the optimized parameters are reasonably robust within typical parameter variations.
244 We also tested the clustering parameters under random noise conditions by introducing noise.
245 When adding Gaussian noise to the data (see Methods), no noise-iterated dataset (n = 1,000)

246 produced a silhouette score higher than the observed silhouette from the original clustering,
247 resulting in an empirical p-value of 0.008. This indicates that the cluster structure reflects
248 meaningful biological separation rather than random fluctuations. Notably, the silhouette score
249 exhibited only 6% degradation under this noise level, indicating cluster stability.

250 A total of 185 genes significantly differentiated between M_1 and M_2 cells (obtained from
251 Wilcoxon Rank Sum test; see Methods). The genes that contributed the most to the genetic
252 variance between M_1 and M_2 cells are illustrated in the heatmap of Figure 2D, showing the
253 expression levels of the most differential genes (top 10 genes from each population ranked by
254 ascending adjusted *p*-value) for each cell. Genes of particular interest from our ontology analysis
255 are shown in the dot and volcano plots (Figure 2E and 2F, respectively).

256 Generally, from our ontology, M_1 cells show upregulation of genes associated with action
257 potentials and signal transmission whereas M_2 cells express cytoskeletal/intracellular transport
258 proteins and genes involved in transcription and post-transcription regulation. Notably enriched
259 genes in M_1 cells include GRIK2 (ionotropic kainate-type glutamate receptor subunit) and
260 GRM1 (metabotropic glutamate receptor), alongside a diverse array of voltage-gated potassium
261 channel subunits (KCNC2, KCND2, KCNJ3, KCNH5) and the voltage-gated calcium channel
262 auxiliary subunit CACNA2D1. Conversely, M_2 cells express microtubule-associated proteins
263 such as MAP1A and MAPT, which stabilize dendritic and axonal microtubules respectively,
264 alongside cytoskeletal components SPTAN1, SPTBN2, and TTN. In addition, M_2 cells express
265 transcriptional regulators including KMT2B, a histone methyltransferase that modulates
266 chromatin architecture and gene expression; SRRT, an RNA-binding protein involved in miRNA
267 processing; and SNAPC4, a component of the snRNA-activating complex essential for snRNA
268 transcription and RNA processing. Finally, M_2 cells exhibit high levels of genes involved in

intracellular transport and cytoskeletal signaling. For example, KIF1A and KIFC2 encode kinesin motor proteins that mediate anterograde and retrograde vesicular transport along microtubules, while MAST1 encodes a microtubule-associated serine/threonine kinase implicated in regulating synapse-associated cytoskeletal dynamics (Tripathy et al., 2018).

Overall, the mild degree of genetic differentiation is consistent with the modest silhouette scores and the lack of sharply distinct clustering in UMAP space. This subtle separation could suggest that M_1 and M_2 represent a gradient or continuum of transcriptional subtypes rather than discrete populations. It is also noteworthy that the original work of Bakken et al. (2021) did not identify subtypes within magnocellular neurons, suggesting that the M1/M2 split observed in the current study likely arises from the increased sensitivity of our clustering optimization pipeline (more in the Discussion), although only detecting modest transcriptomic divergence. In summary, while transcriptomic evidence supports the existence of two subpopulations within M cells, the limited biological separation indicates that these likely reflect subtle molecular differences rather than robustly distinct cell types.

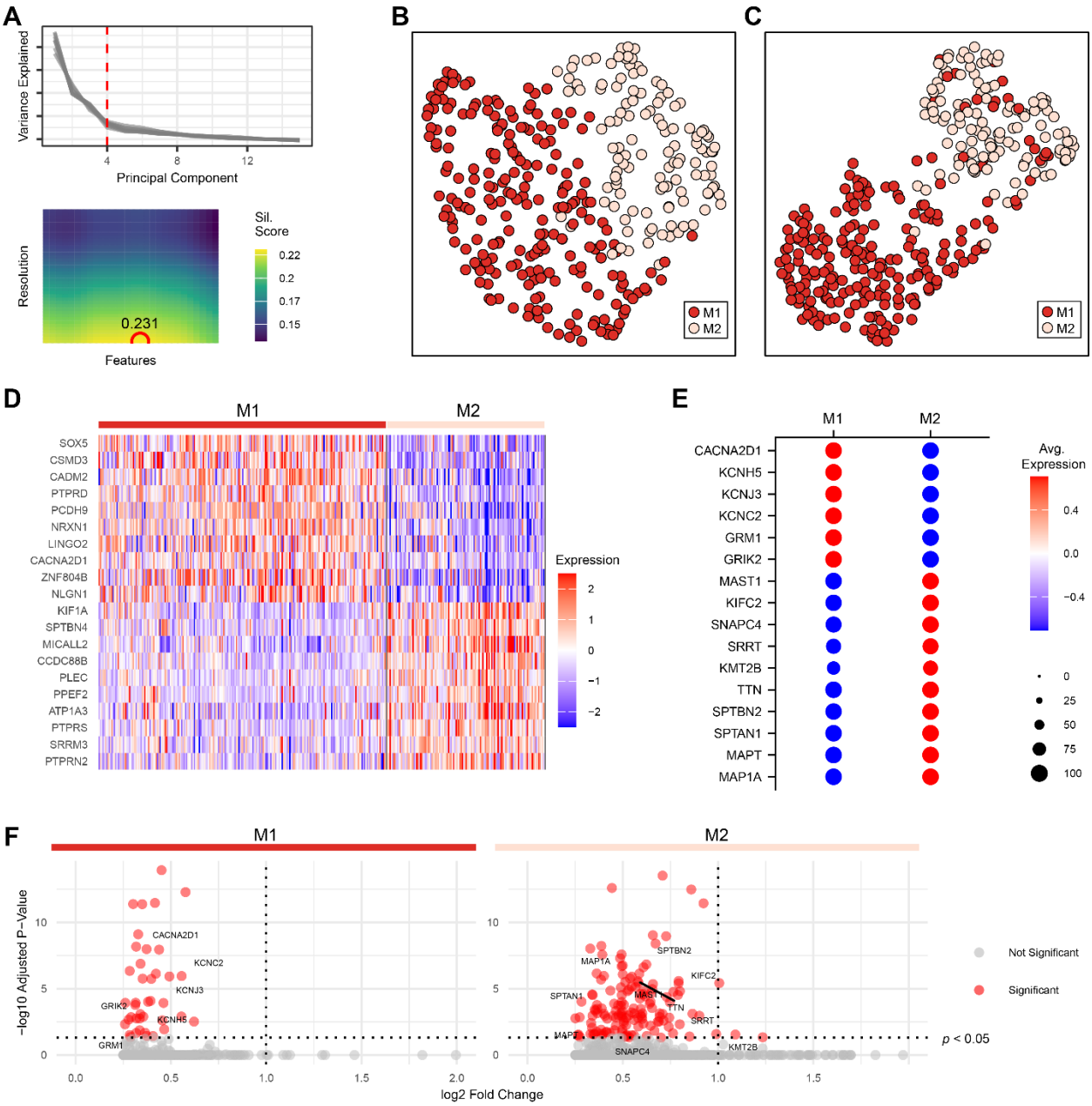

Figure 2. M cell clustering produced two clusters: M_1 (n = 226, red) and M_2 (n = 124, light-red). (**A**) Top, elbow plot to qualitatively determine the number of PCs at the elbow (red dashed line). Bottom, heat map of GAM-fitted silhouette scores from varying combinations of number of high variable features and clustering resolution (bottom). The red circle in the heat map indicates the maximum predicted silhouette score. The optimum number of PCs, high variable features, and clustering resolution were used for downstream analysis. **(B)** Scatter plot visualization of M_1 and

291 M_2 clusters in UMAP space from the parameters determined in A. **(C)** The same UMAP plot but
292 only using the differentially expressed genes between M_1 and M_2 clusters (adjusted *p*-value <
293 0.05, *n* = 185). (**D**) Heatmap of RNA-seq expression for the top 10 differentially expressed genes
294 (ordered by increasing adjusted *p*-value; positive fold change only) for each cluster. The
295 horizontal and vertical axes represent individual cells and differentially expressed genes,
296 respectively. The colored bars on the top and left of the plot represent the cells and the top 10
297 differentially expressed for each cluster, respectively. The legend on the right describes the
298 expression levels for each gene and cell. (**E**) Gene expression dot plot showing the expression of
299 notable M_1 and M_2 significant markers (adjusted *p*-value < 0.05). Dot diameter indicates the
300 proportion of cells expressing the gene, and color intensity indicates average expression levels.
301 **(F)** Volcano plot of differential gene expression between M_1 and M_2 clusters. The x-axis
302 represents the fold change in expression, and the y-axis represents the –log10 adjusted p-value.
303 Genes passing significance threshold (adjusted p-value < 0.05) are represented as red data points.
304 The genes featured in E are labelled for reference.

305

306 **P cell clustering**

307 Similarly, two subpopulations were identified within P cells: P_1 (n = 334) and P_2 (n =
308 291). The optimized parameters were 4 PCs, 3200 top features, and a clustering resolution of
309 0.26 (Figure 3A) with a 0.225 silhouette score for this clustering, indicating a low to moderate
310 separation as visualized in the UMAP plot (Figure 3B). Restricting to the set of significant genes
311 (n = 692) improves the clustering to a moderate separation with a silhouette score of 0.329
312 (Figure 3C). Cluster sensitivity testing yielded a moderate cluster reproduction with 55% of

313 iterations matching two P clusters with an average cluster identity match of 82.3 ± 9.4%.
314 Clustering stability testing, adding gaussian noise to the data, resulted in a silhouette score
315 degradation by only 5.88% with no noisy data iteration with a higher silhouette score than the
316 original (empirical *p*-value of 0.000), indicating that the clustering reflects meaningful biological
317 signal rather than noise.

318 A total of 692 genes were significantly differentially expressed between P_1 and P_2
319 (adjusted $p < 0.05$), with 625 genes enriched in P_1 and 67 in P_2. The most significant genetic
320 differences contributing to the P_1 and P_2 separation are illustrated in the heatmap of Figure 3D,
321 and genes of particular interest in our ontology are shown in the plots of Figure 3E and 3F.

322 From our ontology, P_1 cells express multiple components of the mitochondrial electron
323 transport chain complex I, including NDUFA11, NDUFV1, and NDUFS8, as well as glycolytic
324 enzymes such as TPI1 (triosephosphate isomerase) and GAPDH (glyceraldehyde-3-phosphate
325 dehydrogenase). The mitochondrial GTP-binding protein GTPBP6, implicated in proper
326 mitochondrial translation and oxidative phosphorylation (Lavdovskaia et al., 2020) and STK11, a
327 master regulator of cellular metabolism and energy homeostasis (Huang & Li, 2022), are also
328 highly expressed. In parallel, P_1 cells express a number of genes that afford protection against
329 oxidative and metabolic stress. These include HSPB1, HSP90AB1, and HSPA12A – heat shock
330 proteins known to stabilize cytoskeletal and synaptic proteins under stress (Dávila et al., 2014;
331 Toth et al., 2010; Wang et al., 2023); NUDT1, which prevents mutagenesis by hydrolyzing
332 oxidized nucleotides; BOK, a BCL-2 family protein involved in mitochondrial dynamics and
333 endoplasmic reticulum stress responses independent of apoptosis (D'Orsi et al., 2016); and
334 MAP4K2, an upstream activator of the JNK pathway, which is a 'cell death' pathway involved
335 in cellular stress signaling (Weston & Davis, 2007). Finally, P_1 cells express a number of ion

channels, including SCN2B (voltage-gated sodium channel subunit), KCNT1, KCNAB2, KCNC1, KCNJ12, KCNK3, KCNQ1, KCNQ2 (potassium ion channel subunits), CACNA1G, CACNA1A, CNCBA1B, CACNA1C (voltage-gated calcium channel subunits), and GRIN1 (glutamate NMDA receptor subunit).

By contrast, P_2 cells express genes such as NRXN1 (neurexin 1) and NLGN1 (neuroligin 1) which, as a pair, function as cell adhesion molecules which bind with each other to establish excitatory/inhibitory synapse specificity (Arias-Aragón et al., 2025; Gomez et al., 2021). NLGN1 specifically promotes excitatory glutamatergic synapse formation (Szíber et al., 2024; Zeidan & Ziv, 2012). NRG3 (neuroregulin) is likewise involved in the formation of excitatory synapses (Müller et al., 2018). CDH2, PCDH7, PCDH9 are all members of the cadherin superfamily, playing roles in axon pathfinding, synaptic targeting, and circuit refinement.

Overall, P_1 cells show high expression of genes associated with cellular metabolism and energy production, especially aerobic metabolism, as well as a number of genes responsible for protecting the cell from oxidative and metabolic stressors. P_2 cells, by contrast, express genes important for synaptic regulation and specificity, cell adhesion, and calcium signaling – suggesting an emphasis on connectivity and plasticity.

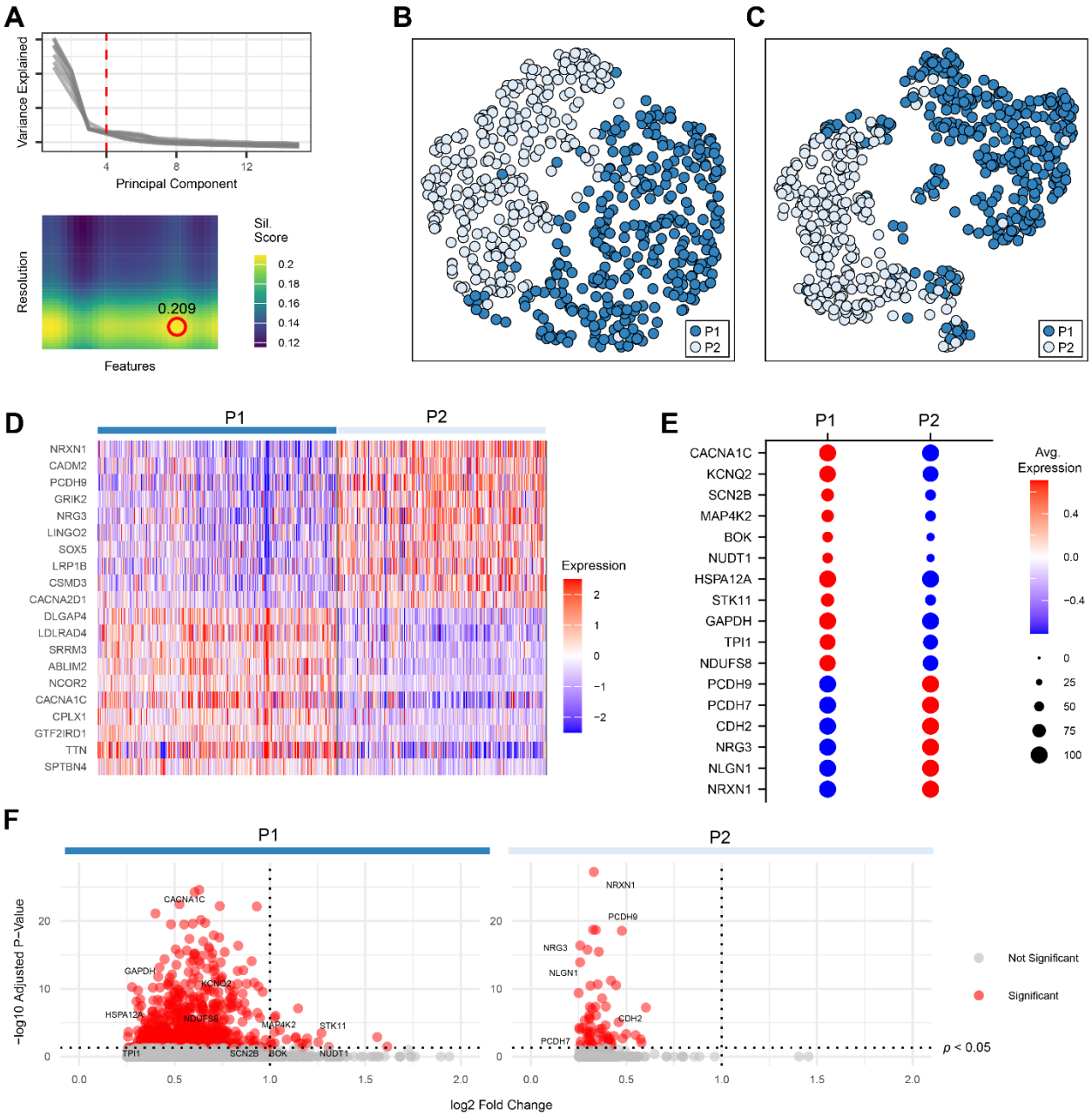

Figure 3. P cell clustering produced two clusters: P_1 (n = 334; dark blue) and P_2 (n = 291; light blue). **(A)** Top, elbow plot to qualitatively determine the number of PCs at the elbow (red dashed line). Bottom, heat map of GAM-fitted silhouette scores from varying combinations of number of highly variable features and clustering resolution. The redcircle in the heat map marks the optimal parameters used in downstream analysis. **(B)** Scatter plot visualization of P_1 and P_2 clusters in UMAP space using the parameters from A. **(C)** The same UMAP plot restricted to

differentially expressed genes between P_1 and P_2 (adjusted *p*-value < 0.05, *n* = 692). **(D)** Heatmap of RNA-seq expression for the top 10 differentially expressed genes (ordered by increasing adjusted *p*-value; positive fold change only) for each cluster. Horizontal and vertical axes represent individual cells and genes, respectively. Colored bars denote cluster identity. **(E)** Gene expression dot plot showing expression of notable significant markers in P_1 and P_2. Dot diameter represents the proportion of cells expressing the gene; color intensity reflects average expression. **(F)** Volcano plot showing fold change versus –log10 adjusted *p*-value for each gene. Genes meeting both statistical and biological significance are highlighted in red, with markers from **(E)** labeled.

K cell clustering

The K cell population exhibited a stronger degree of transcriptional heterogeneity in contrast to P and M cells. Three subpopulations were identified: K_1 (n = 151), K_2 (n = 120), and K_3 (n = 63). The optimized parameters we obtained for K clusters were 4 PCs, 1100 top features, and a clustering resolution of 0.12 (Figure 4A), achieving a stronger silhouette score of 0.401. Using only the significant genes (n = 642) yielded only a slightly higher silhouette score of 0.42 (Figure 4C). The K clustering also produced high stability with an average cluster reproduction match of 92.1 ± 4.5% (*n* = 1000; 14.2% skipped due to cluster mismatch). Noise testing produced an empirical *p*-value of 0.001, with a silhouette degradation of 6.96%, further confirming the robustness of the clustering.

382 A total of 642 genes were significantly differentially expressed across the K clusters
383 (adjusted $p < 0.05$), with 66 enriched in K_1, 186 in K2, and 390 in K3. Of these, 361 genes met
384 biological significance criteria, including 16 in K_1, 76 in K2, and 269 in K3 (Figures 4D). This
385 distribution highlights the substantial heterogeneity within the K population, particularly the
386 strong separation of K_3. Genes of particular interest in our ontology are shown in the plots of
387 Figure 4E and 4F, and described below.

388 All three K cell subpopulations (K_1, K_2, K_3) express ion channels and glutamate receptors
389 needed for signal transmission and action potential generation, though with subtle functional
390 differences. In addition, coexpression of other genes (such as Ca^{2+}-ATPases in K_1, cytoskeletal
391 binding elements in K_2, and non-glutamate receptors in K_3) highlights distinct roles for each
392 subpopulation.

393 Key genes expressed by K_1 cells include ion channel subunits such as KCNC2, KCNN3,
394 KCNB2, and CACNA1I, as well as ATP1B2, a subunit of the Na^+/K^+-ATPase critical for
395 maintaining resting membrane potential. Notably, K_1 cells selectively express metabotropic
396 glutamate receptor subunits GRM5 and GRM7, G protein-coupled receptors that mediate slower,
397 modulatory synaptic responses via second messenger cascades. K_1 cells also express ATP2A3
398 and ATP2B1, which encode plasma membrane and endoplasmic reticulum Ca^{2+}-ATPases
399 involved in calcium extrusion and intracellular calcium homeostasis.

400 K_2 cells also express a number of proteins important in signal transmission,
401 including KCNH1, KCNJ3, KCNAB3, SCN1B, SCN9A (sodium and potassium ion channel
402 subunits) and GRIK4, GRIA4 (ionotropic kainate and AMPA glutamate receptors). However, in
403 addition to those proteins important for signal transmission are also a substantial number of

404 proteins involved in cytoskeletal binding, including TTN, TNS1, FMN1, MTUS1, SPTB,
405 MYLK, MYO5B, MYO16, MYO19, MYO14.

406 The K_3 population of cells expresses a large number of monoatomic ion channels,
407 channels important for electrical signaling in neurons. These include KCNIP1, KCNA3,
408 KCNQ1, KCNQ5, KCNC4, KCNJ6, KCNK2, KCNK3, KCNH3, KCNT2, KCNK10, KCNMA1
409 (subunits of different potassium channels, including voltage-gated, sodium-activated, two-pore
410 domain, and inwardly rectifying types), CACNA1E, CACNA1B, and CACNG4 (voltage-gated
411 calcium channel subunits). In addition to these ion channels, this cell population expresses a
412 substantial amount of neurotransmitter receptors for both glutamate – the primary excitatory
413 neurotransmitter in LGN – as well as other modulatory neurotransmitters. These include GRID1,
414 GRID2, GRIN3A, GRM2, GRIK5 (glutamate receptors; NMDA, delta, and kainate type), HRH1
415 (histamine H1 receptor), OPRK1 (opioid receptor kappa), MGLL (endocannabinoid related
416 lipase), TRPM3 (neurosteroid sensitive transient receptor potential channel; Webster et al.,
417 2020), CHRNA7 (nicotinic acetylcholine receptor subunit), and P2RX4 (purinergic receptor).

418 In the current analysis, the Kp and Kap cells from Bakken et al. (2021) were analyzed
419 and clustered together due to the relatively small number of Kap cells. Despite this, the
420 clustering from the current analysis consistently grouped Kap cells into K_3, while subdividing the
421 remaining Kp cells into K_1 and K_2. A supplementary figure (Supplementary Figure 2) confirms
422 that K_3 aligns with the Kap identity (90%, n = 66/73), indicating that the Kap population is
423 preserved and identifiable within the revised clustering framework.

424 Overall, the strong degree of genetic differentiation within the K population is reflected
425 in the ontology, higher silhouette scores, and clear separation in UMAP space. The dominant

426 transcriptomic signature of K_3, along with the high number of biologically significant genes,
427 suggests that K_1, K_2, and K_3 represent robust and distinct molecular subtypes. This result refines
428 the earlier findings of Bakken et al. (2021), which identified Kp and Kap subtypes, by further
429 subdividing Kp into K_1 and K_2 while preserving Kap as K_3. The transcriptomic evidence
430 supports the existence of three distinct subpopulations within K cells, indicating a greater degree
431 of heterogeneity in the koniocellular pathway compared to the magnocellular and parvocellular
432 pathways.

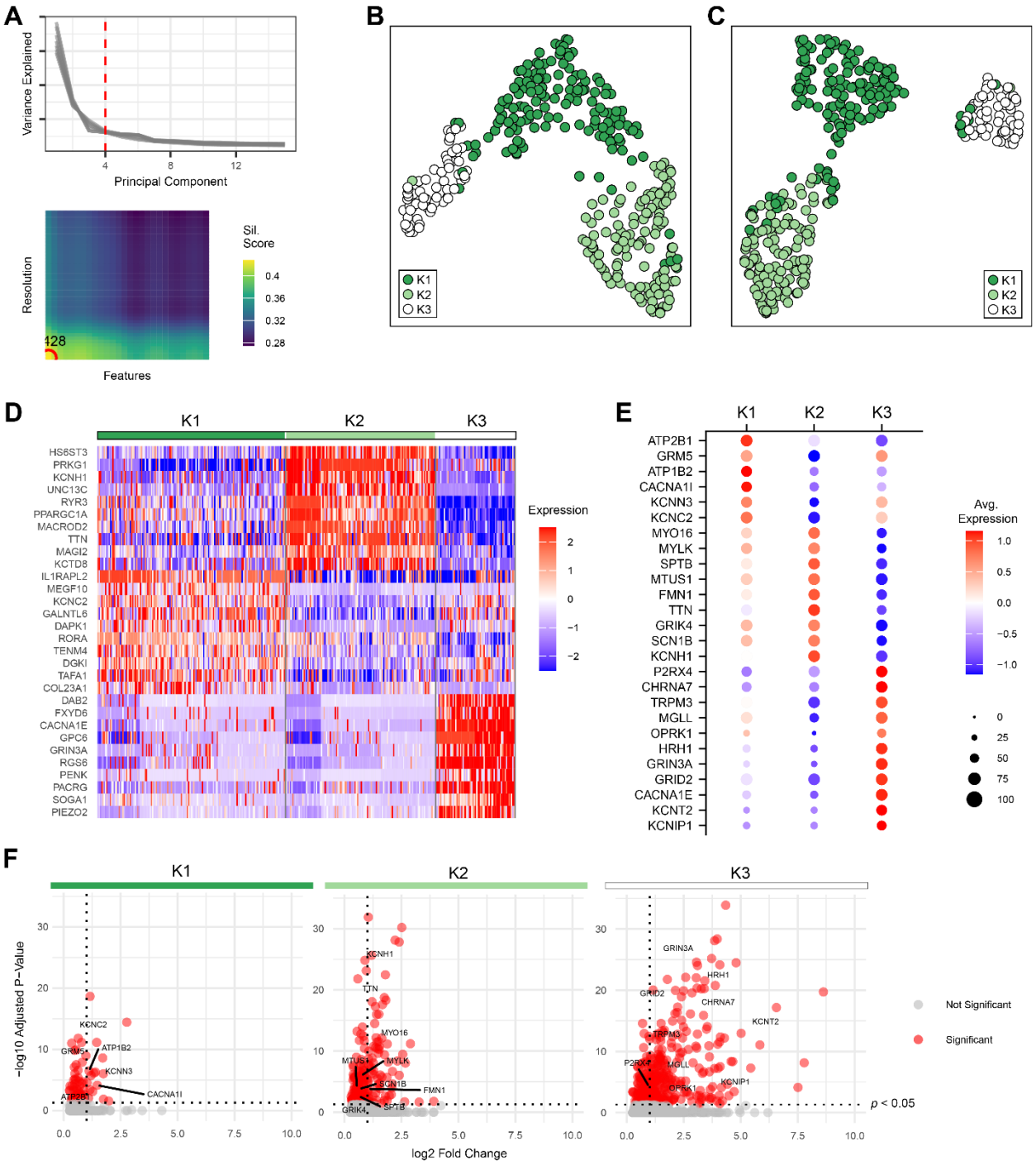

433

434 **Figure 4.** K cell clustering produced four clusters: K_1 (n = 151; dark green), K_2 (n = 120; light

435 green), and K_3 (n = 63; white). **(A)** Top, elbow plot used to determine the number of PCs at the

436 elbow (red dashed line). Bottom, heat map of GAM-fitted silhouette scores across combinations

437 of feature number and clustering resolution. The red circle indicates the optimum parameter set.

(B) UMAP visualization of K_1, K_2, and K_3 clusters using the parameters in A. **(C)** UMAP using only differentially expressed genes between clusters (adjusted *p*-value < 0.05, *n* = 642). **(D)** Heatmap of RNA-seq expression for the top 10 differentially expressed genes (ordered by increasing adjusted *p*-value; positive fold change only) per cluster. Axes indicate individual cells and gene markers; color bars denote cluster identity. **(E)** Gene expression dot plot showing notable markers in each K cluster. Dot size corresponds to expression frequency; color intensity to average expression level. **(F)** Volcano plot of differential gene expression across clusters. X-axis denotes fold change; Y-axis, –log10 adjusted *p*-value. Genes from **(E)** are labeled.

Interspecies and donor variability

To assess whether the observed subpopulations were confounded by interspecies differences or individual subject variability, we performed a qualitative evaluation of UMAP plots for the M, P, and K populations colored by individual animal (*n* = 3) and species (*M. fascicularis* and *M. nemestrina*) (Supplementary Figure 3). As shown in these plots, the major subpopulations are preserved across both subject and species. To quantify this observation, we performed Fisher's exact tests to evaluate species and subject enrichment within each cluster. No species enrichment was observed in any cluster after Bonferroni correction ($p > 0.05$), indicating that interspecies differences did not drive the clustering. Similarly, no donor enrichment was detected in any of the clusters, except for one koniocellular cluster, K3. K3 exhibited significant donor enrichment ($p = 0.00023$; $p_adj = 0.0033$), likely reflecting the relatively small size of the K3 population. Taken together, these results suggest that the M, P, and K subpopulations are not driven by species- or subject-related differences, and reflect underlying biological distinctions.

Subtype	**Key Gene Expression**	**Functional Implications**
M_1	- Ionotropic (GRIK2) & metabotropic (GRM1) glutamate receptors - Voltage-gated potassium channels (KCNC2, KCND2, KCNJ3, KCNH5) - Voltage-gated calcium channel subunit (CACNA2D1)	- Optimized for rapid, high-fidelity signal transmission - Fast, phasic relay neurons - Fast excitability and spike timing regulation
M_2	- Cytoskeletal proteins (MAP1A, MAPT, SPTAN1, SPTBN2, TTN) - Transcriptional regulators (KMT2B, SRRT, SNAPC4) - Kinesin motor proteins (KIF1A, KIFC2) - Microtubule-associated kinase (MAST1)	- Structurally robust, adapted for synaptic plasticity - Modulatory role integrating feedforward and feedback inputs - Supports synaptic remodeling and network activity

P_1	- Mitochondrial ETC components (NDUFA11, NDUFV1, NDUFS8) - Glycolytic enzymes (TPI1, GAPDH) - Metabolic regulators (GTPBP6, STK11) - Heat shock proteins (HSPB1, HSP90AB1, HSPA12A) - Ion channels (SCN2B, KCNT1, KCNAB2, etc.) - NMDA receptor subunit (GRIN1)	- High metabolic activity and oxidative stress protection - Tonic firing, high-fidelity relay neurons - Sustained firing patterns suitable for detailed vision
P_2	- Synaptic adhesion molecules (NRXN1, NLGN1) - Cadherins (CDH2, PCDH7, PCDH9) - Calcium signaling genes (NRG3)	- Emphasis on synaptic specificity, plasticity, and connectivity - Modulatory role in circuit refinement and activity-dependent changes
K_1	- Ion channels (KCNC2, KCNN3, KCNB2) - Na^+/K^+-ATPase subunit - Metabotropic glutamate receptors (GRM5, GRM7) - Calcium ATPases (ATP2A3, ATP2B1)	- Slower synaptic response kinetics via metabotropic receptors - High-throughput synaptic activity with calcium regulation

K_2	- Signal transmission proteins (KCNH1, KCNJ3, SCN1B, GRIK4, GRIA4) - Cytoskeletal proteins (TTN, TNS1, FMN1, MTUS1, SPTB, MYLK, MYO family)	- Structurally robust with fast conduction properties - Possible projections to extrastriate areas for reflexive/feedforward processing
K_3	- Numerous potassium channel subunits (KCNIP1, KCNA3, etc.) - Glutamate receptors (GRID1, GRID2, GRIN3A, GRM2, GRIK5) - Non-glutamate receptors (HRH1, OPRK1, MGLL, TRPM3, CHRNA7, P2RX4) - PENK (proenkephalin)	- Highly electrically active, involved in visual modulation by multiple neurotransmitter systems - Respond to arousal, attention, pain, metabolic, and hormonal states

460 **Table 1.** Summary of ontology analysis.

461

462 # Discussion

463 Our transcriptomic analysis revealed seven subpopulations of LGN neurons: two populations of
464 magnocellular neurons (M_1 and M_2), two populations of parvocellular neurons (P_1 and P_2), and
465 three populations of koniocellular neurons (K_1, K_2, and K_3). Although the same dataset was used
466 as Bakken et al. (2021), our study employed several different analytical methods. Notably, we
467 utilized analytic Pearson residuals for normalization (*SCTransform*, Lause *et al.*, 2021),
468 Harmony integration for batch correction (*HarmonyIntegration*; Korsunsky *et al.*, 2019), and a
469 silhouette-based global parameter optimization pipeline, all of which likely enabled the
470 identification of the nuanced subpopulations in the LGN macaque data.

471 Examining the gene expression of M, P, and K subtypes elucidates some interesting
472 themes (see Table 1 for summary). As for M and P cells, there appears to be two distinct
473 populations of neurons: first, a population of neurons with genes optimizing for high-throughput
474 signal transmission. In the high-throughput populations of M and P cells, distinct gene
475 expression patterns suggest differences in signaling kinetics, matching the electrophysiologic
476 response profiles observed for each population (Kaplan & Shapley, 1982; Lee & Sun, 2009;
477 Maunsell et al., 1999). The second population of M and P cells shows a striking absence of
478 proteins essential for signal transmission, including ion channels, glutamate receptors, and
479 metabolic genes. Instead, they seem to serve a more modulatory role, expressing genes involved
480 in synaptic plasticity, connectivity, and cytoskeletal structure.

481 K cells do not exhibit the clear high-throughput vs. modulatory division seen in M and P
482 cells. This aligns with numerous studies describing K cells as a more heterogeneous,
483 biochemically unique, and functionally distinct part of the visual system (Hendry & Reid, 2000;

484 Xu et al., 2001). All K neuron populations express proteins important for signal transmission,
485 however the specific signal transmission proteins upregulated in each population gives insight
486 into the response kinetics of each population and highlights the electrophysiologically observed
487 heterogeneity in response kinetics of K cells (Eiber et al., 2018; White et al., 2001; Xu et al.,
488 2001).

489 Of note, these functional differences of M, P, and K cell populations discussed below
490 come from gene ontology analyses based on a selected subset of expressed genes. While these
491 inferences provide valuable insights, the absence of electrophysiological, morphological, and
492 spatial data limits the ability to comprehensively characterize each cell type.

493 Magnocellular

494 The gene expression profile of M_1 cells suggests that they are specialized for rapid, high-fidelity
495 signal transmission, consistent with a role as fast, excitable relay neurons adapted to process
496 high-throughput glutamatergic input. The co-expression of both ionotropic (GRIK2) and
497 metabotropic (GRM1) glutamate receptors indicates that these cells are highly responsive to
498 glutamatergic input, likely from retinothalamic projections, through both fast inotropic and
499 slower metabotropic modulatory signaling mechanisms. Kainate receptors such as those encoded
500 by GRIK2 activate within <1 ms at high glutamate concentrations, generating rapid excitatory
501 currents, and rapidly deactivate or desensitize as glutamate levels decline or remain elevated,
502 enabling precise temporal transmission of retinal signals (Lerma et al., 1997). In contrast,
503 metabotropic glutamate receptors encoded by GRM1 are G protein-coupled receptors that
504 modulate downstream signaling pathways, potentially allowing for delayed dynamic tuning of
505 neuronal responsiveness over time (Sugiyama et al., 1987).

506 High expression of voltage-gated potassium and calcium channel subunits further
507 supports a role in feedforward, high-throughput synaptic transmission. The expression of
508 multiple potassium channel subtypes suggests finely tuned regulation of excitability and spike
509 timing (reviewed in Jan & Jan, 2012). For instance, KCNC2 encodes a high-threshold, fast-
510 activating potassium channel that enables brief, high-frequency action potentials (Yan et al.,
511 2005), while KCND2 contributes to A-type currents that regulate subthreshold excitability,
512 repetitive firing frequency, and back-propagation of action potentials (Connor & Stevens, 1971;
513 Shibata et al., 2000; Zhang & McBain, 1995). CACNA2D1, an auxiliary subunit of voltage-
514 gated calcium channels, enhances calcium channel trafficking and function, supporting efficient
515 neurotransmitter release and dendritic integration. Together, these expression patterns reinforce
516 the hypothesis that M_1 cells function as fast-acting, phasic relay neurons within the LGN,
517 aligning with the classical view of magnocellular pathways as mediators of high-speed visual
518 processing (Kaplan & Shapley, 1982; Maunsell et al., 1999).

519 M_2 cells, in contrast to M_1 cells, appear structurally robust and preferentially adapted for
520 synaptic plasticity rather than high-throughput signal relay. Their gene expression profile
521 suggests a potential role as modulatory hubs with context-dependent outputs, potentially
522 mediated through dynamic regulation of receptor composition, axonal targeting, or synaptic
523 scaffolding. Notably, M_2 cells show enriched expression of genes involved in cytoskeletal
524 architecture, intracellular transport, and transcriptional/post-transcriptional regulation. These
525 expression patterns suggest ongoing transcriptional remodeling, possibly in response to activity-
526 dependent plasticity or extra-thalamic modulation.

527 Principally, these findings support that M_2 cells are structurally robust. The concerted
528 expression of genes related to cytoskeletal organization, vesicular transport, and transcriptional

529 control – particularly in the relative absence of classical excitability markers such as ionotropic
530 receptors and voltage-gated ion channels – points to two possible, non-mutually exclusive
531 hypotheses regarding M_2 functionality: first, it's possible that the gene expression profile of M_2
532 cells indicates different action potential kinetics from M_1 cells. While M_1 cells are highly
533 excitable, phasic, and fast, M_2 cells may be more structurally robust, but exhibit slower, more
534 sustained kinetics. One source of evidence supporting this hypothesis comes from many
535 laboratories who have demonstrated that, while P cells demonstrate homogeneously sustained
536 kinetics, M cells contains both transient and sustained neurons (Blakemore & Vital-Durand,
537 1986; Kaplan & Shapley, 1982; Levitt et al., 2001; Xu et al., 2001). As a second hypothesis, it's
538 possible that these cells have a specialized role in coordinating synaptic plasticity, integrating
539 feedback and feedforward input, and regulating broader network activity across thalamocortical
540 circuits. M_2 cells may not be built structurally strong because of size, but instead due to a need to
541 coordinate traffic, form many synaptic connections, and modulate activity broadly. Given the co-
542 expression of many transcriptional regulatory proteins, these cells may serve a more integrative
543 role within the LGN, optimized for modulatory functions rather than rapid signal relay.

544 Overall, M cells appear to have two functionally distinct populations. M_1 cells are the
545 prototypically-understood definition of magnocellular neurons. They appear to be the work-
546 horses of electrical transmission, but simple relay neurons, transmitting information from retina
547 to cortex with minimal modulation or refinement. Their presumed response kinetics are the
548 classically understood fast response kinetics and high temporal frequencies associated with M
549 cells. M_2 cells seem to be more modulatory players. With an absence of proteins important for
550 excitability, action potentials, or synaptic transmission, these are structurally robust neurons,
551 possibly with extensive networks of dendrites or axons. Their high expression of proteins

552 involved in transcriptional and post-transcriptional suggests that they have a role in activity- or
553 state-dependent modulation of neural activity. As opposed to simple relay neurons, M_2 neurons
554 may be responsible for visual processing of retinofugal input to LGN.

555 Parvocellular

556 P_1 cells exhibit a gene expression profile marked by high metabolic activity and enhanced
557 resilience to oxidative and mitochondrial stress, suggesting specialization for sustained, energy-
558 demanding function. Among the most biologically significant markers are numerous enzymes
559 involved in core metabolic pathways and cellular stress regulation. Notably, P_1 cells express
560 multiple components of the mitochondrial electron transport chain complex I, as well as
561 glycolytic enzymes. Mitochondrial GTP-binding protein GTPBP6, implicated in proper
562 mitochondrial translation and oxidative phosphorylation (Lavdovskaia et al., 2020) and STK11, a
563 master regulator of cellular metabolism and energy homeostasis (Huang & Li, 2022) support the
564 interpretation that P_1 neurons have high, sustained energy demands, relying heavily on aerobic
565 respiration to maintain function under prolonged activity. Finally, P_1 cells express a number of
566 genes, such as heat shock proteins, NUDT1, BOK, and MAP4K2, that confer protection against
567 oxidative and metabolic stress.

568 To further support the hypothesis that P_1 cells function as a high-throughput population of relay
569 neurons, these cells exhibit robust expression of genes involved in action potential generation
570 and synaptic transmission, paralleling the molecular profile of M_1 cells. These include a voltage-
571 gated sodium channel subunit, potassium ion channel subunits, voltage-gated calcium channel
572 subunits, and glutamate NMDA receptor subunit.

573 This gene expression profile supports the hypothesis that P_1 cells are metabolically robust relay
574 neurons. Like M_1 neurons, P_1 neurons may serve high-throughput relay functions, however the
575 distinctive upregulation of genes associated with oxidative metabolism, mitochondrial integrity,
576 and stress resilience in P_1 cells suggests a tonic firing profile rather than the fast, phasic signaling
577 characteristic of M_1 cells. This aligns with classical physiological descriptions of parvocellular
578 neurons as exhibiting sustained firing patterns in support of detailed, high-fidelity, continuous
579 visual processing (Lee & Sun, 2009; Maunsell et al., 1999).

580 While P_1 cells express proteins suggestive of high-throughput signal transmission, P_2 cells
581 demonstrate gene expression important for synapse formation and specificity, cell adhesion, and
582 calcium signaling, with a notable absence of proteins related to signal transmission – such as ion
583 channels or neurotransmitter receptors. These features suggest a highly plastic and well-
584 connected population of neurons which, like M_2 neurons, may function as a connectional hub or
585 integrator, rather than a high-throughput information relay. Overall, genes such as NRXN1 and
586 NLGN1, as well as multiple members of the cadherin superfamily, suggest that P_2 cells play a
587 role in precision wiring and synaptic specificity, forming highly targeted connections. The
588 expression of activity-regulated structural proteins (e.g., neurexins and neuroligins) may indicate
589 a role in activity-dependent circuit adaptability (Jüngling et al., 2006).

590 Like M cells, P cells also have two functionally distinct populations. P_1 cells (similar to M_1 cells)
591 are the high-throughput signal transmitters with gene expression suggestive of substantial
592 metabolic needs, as well as protection from metabolic stress. These features suggest cells which
593 fire tonically, specific for high-fidelity, high-detail vision. P_2 cells, like M_2 cells, appear to play a
594 more modulatory, information-integration role. They seem to be well connected, with proteins

595 specific for synaptic specificity and involved in activity-dependent structural modulation and
596 regulation.

597 Koniocellular

598 Similar to M_1 and P_1 cell populations, K_1 cells exhibit enriched expression of genes
599 associated with action potential generation and synaptic transmission. However, the specific
600 repertoire of signal transmission proteins in K_1 cells offers insight into their distinct response
601 kinetics and functional specialization relative to M and P neurons. The absence of ionotropic
602 glutamate receptors and the exclusive expression of metabotropic receptors suggest that K_1 cells
603 may exhibit slower synaptic response kinetics, characteristic of the longer response latencies
604 associated with K cells (Pietersen et al., 2014; Xu et al., 2001). These studies also noted highly
605 heterogeneous response kinetics associated with K cells, which is demonstrated by the diversity
606 of different potassium, calcium, sodium, and glutamate receptor types expressed in K_1, K_2, and
607 K_3 cells. The expression of ATP2A3 and ATP2B1, calcium clearance pumps, supports the idea
608 that K_1 cells are equipped to handle high-throughput synaptic activity while minimizing calcium-
609 induced cytotoxicity.

610 In K_2 cells, the presence of cytoskeletal binding proteins suggests that these neurons, like
611 M_2 neurons, are structurally robust. With the coexpression of fast sodium and potassium channel
612 subunits and ionotropic glutamate receptors, one hypothesis is that the upregulation of structural
613 proteins reflects thicker axons with faster conduction velocities, perhaps with projections to
614 extrastriate areas. This implies that K_2 cells could have a role in reflexive behaviors or
615 feedforward signalling, projecting to areas requiring fast, high-bandwidth processing, and could
616 possibly be the basis for observed projections from K layers to MT (Casagrande, 1994; Sincich
617 et al., 2004).

618 The K_3 population of cells expresses many proteins important for electrical signaling in
619 neurons as well as a diverse population of glutamate and non-glutamate neurotransmitter
620 receptors. The increased expression of these genes suggests that this population of cells is highly
621 electrically active and may be the site of visual modulation by non-glutamate neurotransmitter
622 systems within LGN.

623 Like K_1 and K_2 cells, the expression of ion channels and glutamate receptors indicate an
624 active role in signal transmission. The diversity of glutamate receptor types (NMDA, kainate,
625 and delta type ionotropic, as well as metabotropic) and ion channels expressed in K_3 continue to
626 support the electrophysiological findings that K cells overall demonstrate highly heterogeneous
627 response characteristics. The increased expression of potassium ion channels relative to other K
628 subtypes implies that K_3 cells may demonstrate high temporal frequencies similar to M cells – a
629 point to which we will return. However, what is unique about K_3 cells is the vast expression of
630 non-glutamate neurotransmitter receptors. These include receptors specific for histamine,
631 opioids, acetylcholine, extracellular ATP, and lipids/steroids. The expression of these receptors
632 suggest that K_3 cells are under tight top-down and subcortical control; they respond to arousal,
633 attention, alertness, pain, and inflammation, dynamically shifting their output depending on
634 internal brain states (Javadi et al., 2015; Jin et al., 2002; Noseda et al., 2017; Yang et al., 2015).
635 In addition, these neurons may adapt their function in response to steroid hormones, metabolic
636 shifts, or stress, potentially linking vision or sensory processing with hormonal states.

637 The final remark regarding K_3 cells is the expression of PENK (proenkephalin). Bakken
638 et al. (2021) previously performed single-cell RNA sequencing on macaque LGN cells and
639 showed two populations of K cells, Kp and Kap. Kp cells selectively expressed PENK and were
640 enriched in ventral K layers K1 and K2, adjacent to M cells. This association suggests that the K_3

641 cells we identified were the same Kp cells identified by Bakken et al., or a subpopulation thereof,
642 and may help to explain the commonality in response characteristics between M and K_3 cells. In
643 fact, research in the K1 and K2 layers (where these Kp/K_3 cells are enriched) has shown that
644 these cells demonstrate large receptive fields with sensitivity to contrast and high temporal
645 frequencies – very similar to M cell receptive fields (Solomon et al., 2002; White et al., 2001; Xu
646 et al., 2001).

647 Conclusion

648 Overall, the transcriptomic evidence supports a refined view of LGN organization, extending
649 beyond the classical M, P, and K classification. The presence of modest subtypes in M and P
650 pathways and strong molecular heterogeneity in K cells suggests that LGN neurons may play a
651 more diverse and functionally specialized role in visual processing than traditionally held. This
652 heterogeneity could reflect differential involvement in non-visual modulation, temporal
653 dynamics, or attentional processes.

654 Future studies that combine transcriptomics with electrophysiological or anatomical data,
655 such as spatial transcriptomics or patch-seq, will be necessary to validate these subpopulations
656 and clarify their roles. Furthermore, matched functional-transcriptomic datasets would be
657 essential to determine whether any of the transcriptomic clusters observed here correspond to the
658 functionally distinct cells described in recent electrophysiology experiments, to draw further
659 conclusions about the physical organization of the LGN and its rich variety of cell types.

Supplementary Materials

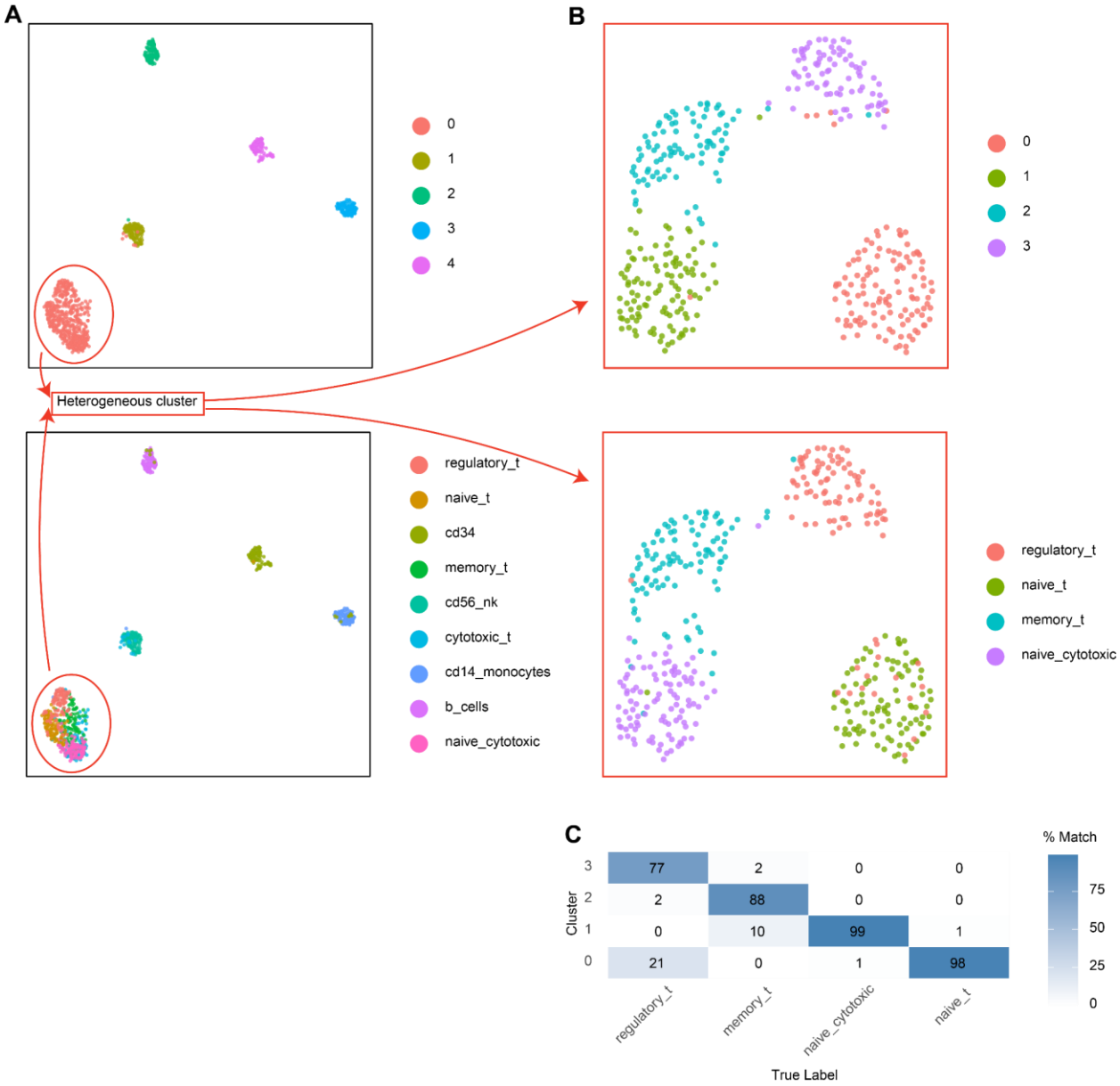

Supplementary Figure 1. Testing the clustering analysis pipeline on ground truth PBMC data. **(A)** UMAPs of clustering using the default Seurat parameters. This produced 5 clusters, including one heterogeneous cluster (bottom-left), when compared to the true labels (bottom UMAP). **(B)** The heterogeneous cluster in A was reclustered using the same clustering pipeline as described in this study (top UMAP). Bottom, the same UMAP plot but labeled using the

growth truth labels. **(C)** Confusion matrix showing match (%) between clusters (y-axis) and true label (x-axis). Overall, the clustering pipeline produced a 90.73% match with the ground truth data.

670 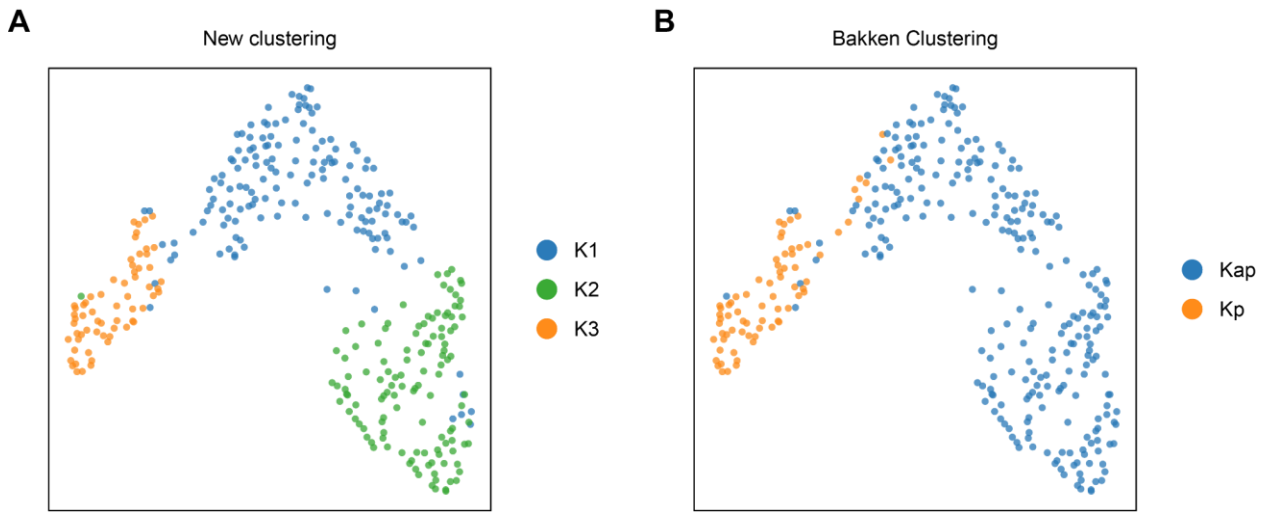

671 **Supplementary Figure 2**. K clustering from the current study **(A)** and from the Bakken et al.

672 (2021) study **(B)**. K3 in the current study is analogous to Kp in the Bakken study with an 86.3%

673 match (n = 63/73).

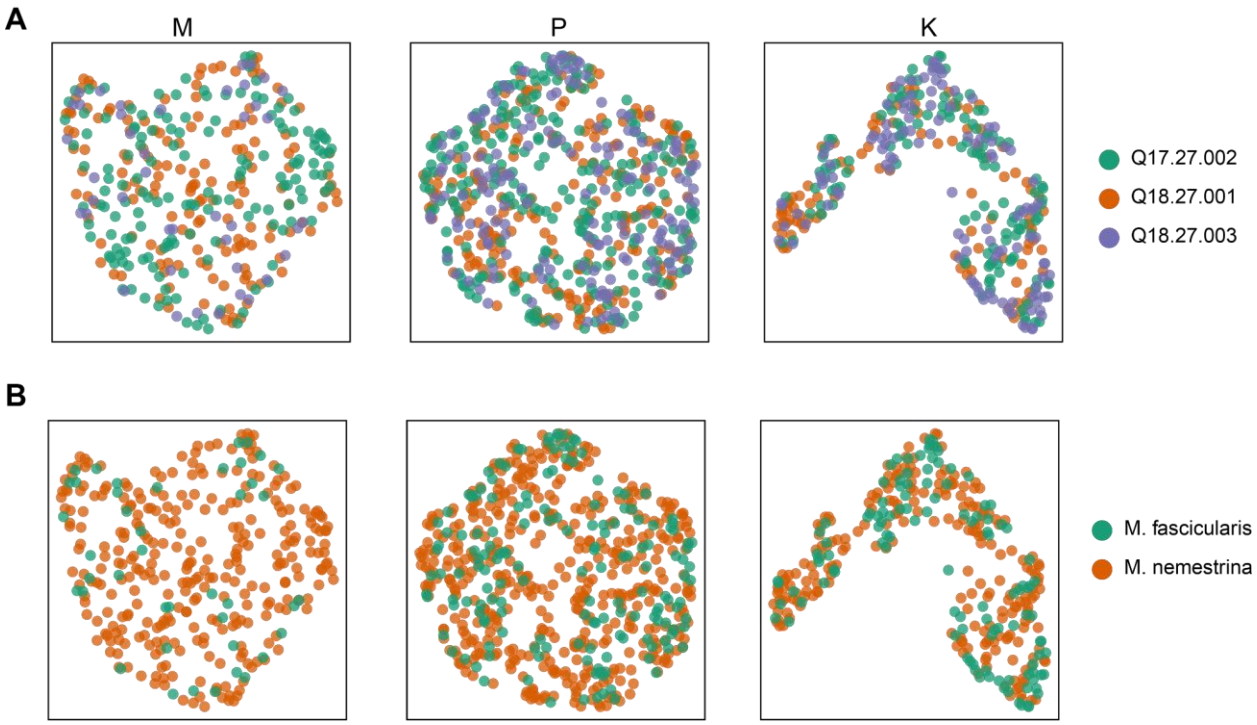

674

675 **Supplementary Figure 3.** The UMAPs of M (left), P (middle), and K clusters (right) with the

676 data labelled by animal id (**A**, n = 3) and species (**B**, n = 2).

Data and Code Availability

The R scripts used for data preprocessing, clustering, and analysis in this study are available online at https://github.com/shihaisun-scott/sun_LGN_macaque_transcriptomics.

680

681 # References

682 Allen Institute for Brain Science. (2022). *Single-cell RNAseq of LGN of mouse, human, and*
683 *nonhuman primate [dataset]* [Dataset]. knowledge.brain-
684 map.org/data/MR9M3L8BU9PCOH3BHCV/summary
685 Arbatsky, M., Vasilyeva, E., Sysoeva, V., Semina, E., Saveliev, V., & Rubina, K. (2025). Seurat
686 function argument values in scRNA-seq data analysis: Potential pitfalls and refinements
687 for biological interpretation. *Frontiers in Bioinformatics*, *5*, 1519468.
688 https://doi.org/10.3389/fbinf.2025.1519468
689 Arias-Aragón, F., Robles-Lanuza, E., Sánchez-Gómez, Á., Martinez-Mir, A., & Scholl, F. G.
690 (2025). Analysis of neurexin-neuroligin complexes supports an isoform-specific role for
691 beta-neurexin-1 dysfunction in a mouse model of autism. *Molecular Brain*, *18*(1), 20.
692 https://doi.org/10.1186/s13041-025-01183-0
693 Bakken, T. E., Hodge, R. D., Miller, J. A., Yao, Z., Nguyen, T. N., Aevermann, B., Barkan, E.,
694 Bertagnolli, D., Casper, T., Dee, N., Garren, E., Goldy, J., Graybuck, L. T., Kroll, M.,
695 Lasken, R. S., Lathia, K., Parry, S., Rimorin, C., Scheuermann, R. H., … Tasic, B.
696 (2018). Single-nucleus and single-cell transcriptomes compared in matched cortical cell
697 types. *PLOS ONE*, *13*(12), e0209648. https://doi.org/10.1371/journal.pone.0209648
698 Bakken, T. E., van Velthoven, C. T., Menon, V., Hodge, R. D., Yao, Z., Nguyen, T. N.,
699 Graybuck, L. T., Horwitz, G. D., Bertagnolli, D., Goldy, J., Yanny, A. M., Garren, E.,
700 Parry, S., Casper, T., Shehata, S. I., Barkan, E. R., Szafer, A., Levi, B. P., Dee, N., …
701 Tasic, B. (2021). Single-cell and single-nucleus RNA-seq uncovers shared and distinct

axes of variation in dorsal LGN neurons in mice, non-human primates, and humans. *eLife*, *10*, e64875. https://doi.org/10.7554/eLife.64875

Blakemore, C., & Vital-Durand, F. (1986). Organization and post-natal development of the monkey's lateral geniculate nucleus. *The Journal of Physiology*, *380*, 453–491. https://doi.org/10.1113/jphysiol.1986.sp016297

Butler, A., Hoffman, P., Smibert, P., Papalexi, E., & Satija, R. (2018). Integrating single-cell transcriptomic data across different conditions, technologies, and species. *Nature Biotechnology*, *36*(5), 411–420. https://doi.org/10.1038/nbt.4096

Casagrande, V. A. (1994). A third parallel visual pathway to primate area V1. *Trends in Neurosciences*, *17*(7), 305–310. https://doi.org/10.1016/0166-2236(94)90065-5

Chen, W., Zhu, X. H., Thulborn, K. R., & Ugurbil, K. (1999). Retinotopic mapping of lateral geniculate nucleus in humans using functional magnetic resonance imaging. *Proceedings of the National Academy of Sciences of the United States of America*, *96*(5), 2430–2434. https://doi.org/10.1073/pnas.96.5.2430

Cheong, S. K., Tailby, C., Solomon, S. G., & Martin, P. R. (2013). Cortical-Like Receptive Fields in the Lateral Geniculate Nucleus of Marmoset Monkeys. *Journal of Neuroscience*, *33*(16), 6864–6876. https://doi.org/10.1523/JNEUROSCI.5208-12.2013

Choudhary, S., & Satija, R. (2022). Comparison and evaluation of statistical error models for scRNA-seq. *Genome Biology*, *23*(1), 27. https://doi.org/10.1186/s13059-021-02584-9

Clarke, Z. A., Andrews, T. S., Atif, J., Pouyabahar, D., Innes, B. T., MacParland, S. A., & Bader, G. D. (2021). Tutorial: Guidelines for annotating single-cell transcriptomic maps using automated and manual methods. *Nature Protocols*, *16*(6), 2749–2764. https://doi.org/10.1038/s41596-021-00534-0

725 Connor, J. A., & Stevens, C. F. (1971). Voltage clamp studies of a transient outward membrane
726 current in gastropod neural somata. *The Journal of Physiology*, *213*(1), 21–30.
727 https://doi.org/10.1113/jphysiol.1971.sp009365
728 Dacey, D. (2004). Origins of perception: Retinal Ganglion Cell Diversity and the Creation of
729 Parallel Visual Pathways. In *Sensory Systems* (pp. 281–301).
730 Dávila, D., Jiménez-Mateos, E. M., Mooney, C. M., Velasco, G., Henshall, D. C., & Prehn, J. H.
731 M. (2014). Hsp27 binding to the 3'UTR of bim mRNA prevents neuronal death during
732 oxidative stress-induced injury: A novel cytoprotective mechanism. *Molecular Biology of*
733 *the Cell*, *25*(21), 3413–3423. https://doi.org/10.1091/mbc.E13-08-0495
734 Denison, R. N., Vu, A. T., Yacoub, E., Feinberg, D. A., & Silver, M. A. (2014). Functional
735 mapping of the magnocellular and parvocellular subdivisions of human LGN.
736 *NeuroImage*, *102*, 358–369. https://doi.org/10.1016/j.neuroimage.2014.07.019
737 Dobin, A., Davis, C. A., Schlesinger, F., Drenkow, J., Zaleski, C., Jha, S., Batut, P., Chaisson,
738 M., & Gingeras, T. R. (2013). STAR: Ultrafast universal RNA-seq aligner.
739 *Bioinformatics*, *29*(1), 15–21. https://doi.org/10.1093/bioinformatics/bts635
740 D'Orsi, B., Engel, T., Pfeiffer, S., Nandi, S., Kaufmann, T., Henshall, D. C., & Prehn, J. H. M.
741 (2016). Bok Is Not Pro-Apoptotic But Suppresses Poly ADP-Ribose Polymerase-
742 Dependent Cell Death Pathways and Protects against Excitotoxic and Seizure-Induced
743 Neuronal Injury. *The Journal of Neuroscience: The Official Journal of the Society for*
744 *Neuroscience*, *36*(16), 4564–4578. https://doi.org/10.1523/JNEUROSCI.3780-15.2016
745 Eiber, C. D., Rahman, A. S., Pietersen, A. N. J., Zeater, N., Dreher, B., Solomon, S. G., &
746 Martin, P. R. (2018). Receptive Field Properties of Koniocellular On/Off Neurons in the

Lateral Geniculate Nucleus of Marmoset Monkeys. *Journal of Neuroscience*, *38*(48), 10384–10398. https://doi.org/10.1523/JNEUROSCI.1679-18.2018

Fu, S., Wang, S., Si, D., Li, G., Gao, Y., & Liu, Q. (2025). Benchmarking single-cell multi-modal data integrations. *Nature Methods*, 1–12. https://doi.org/10.1038/s41592-025-02737-9

Gomez, A. M., Traunmüller, L., & Scheiffele, P. (2021). Neurexins: Molecular Codes for Shaping Neuronal Synapses. *Nature Reviews. Neuroscience*, *22*(3), 137–151. https://doi.org/10.1038/s41583-020-00415-7

Hao, Y., Stuart, T., Kowalski, M. H., Choudhary, S., Hoffman, P., Hartman, A., Srivastava, A., Molla, G., Madad, S., Fernandez-Granda, C., & Satija, R. (2024). Dictionary learning for integrative, multimodal and scalable single-cell analysis. *Nature Biotechnology*, *42*(2), 293–304. https://doi.org/10.1038/s41587-023-01767-y

Hendry, S. H. C., & Reid, R. C. (2000). The Koniocellular Pathway in Primate Vision. *Annual Review of Neuroscience*, *23*(Volume 23, 2000), 127–153. https://doi.org/10.1146/annurev.neuro.23.1.127

Hodge, R. D., Bakken, T. E., Miller, J. A., Smith, K. A., Barkan, E. R., Graybuck, L. T., Close, J. L., Long, B., Johansen, N., Penn, O., Yao, Z., Eggermont, J., Höllt, T., Levi, B. P., Shehata, S. I., Aevermann, B., Beller, A., Bertagnolli, D., Brouner, K., … Lein, E. S. (2019). Conserved cell types with divergent features in human versus mouse cortex. *Nature*, *573*(7772), Article 7772. https://doi.org/10.1038/s41586-019-1506-7

Huang, E., & Li, S. (2022). Liver Kinase B1 Functions as a Regulator for Neural Development and a Therapeutic Target for Neural Repair. *Cells*, *11*(18), 2861. https://doi.org/10.3390/cells11182861

770 Hubel, D. H., & Livingstone, M. S. (1990). Color and contrast sensitivity in the lateral geniculate
771 body and primary visual cortex of the macaque monkey. *The Journal of Neuroscience:*
772 *The Official Journal of the Society for Neuroscience*, *10*(7), 2223–2237.
773 https://doi.org/10.1523/JNEUROSCI.10-07-02223.1990
774 Ichinose, T., & Habib, S. (2022). On and off signaling pathways in the retina and the visual
775 system. *Frontiers in Ophthalmology*, *2*, 989002.
776 https://doi.org/10.3389/fopht.2022.989002
777 Jan, L. Y., & Jan, Y. N. (2012). Voltage-gated potassium channels and the diversity of electrical
778 signalling. *The Journal of Physiology*, *590*(11), 2591–2599.
779 https://doi.org/10.1113/jphysiol.2011.224212
780 Javadi, P., Bouskila, J., Bouchard, J.-F., & Ptito, M. (2015). The endocannabinoid system within
781 the dorsal lateral geniculate nucleus of the vervet monkey. *Neuroscience*, *288*, 135–144.
782 https://doi.org/10.1016/j.neuroscience.2014.12.029
783 Jin, C. Y., Kalimo, H., & Panula, P. (2002). The histaminergic system in human thalamus:
784 Correlation of innervation to receptor expression. *European Journal of Neuroscience*,
785 *15*(7), 1125–1138. https://doi.org/10.1046/j.1460-9568.2002.01951.x
786 Jüngling, K., Eulenburg, V., Moore, R., Kemler, R., Lessmann, V., & Gottmann, K. (2006). N-
787 Cadherin Transsynaptically Regulates Short-Term Plasticity at Glutamatergic Synapses
788 in Embryonic Stem Cell-Derived Neurons. *The Journal of Neuroscience*, *26*(26), 6968–
789 6978. https://doi.org/10.1523/JNEUROSCI.1013-06.2006
790 Kaplan, E., & Shapley, R. M. (1982). X and Y cells in the lateral geniculate nucleus of macaque
791 monkeys. *The Journal of Physiology*, *330*(1), 125–143.
792 https://doi.org/10.1113/jphysiol.1982.sp014333

Korsunsky, I., Millard, N., Fan, J., Slowikowski, K., Zhang, F., Wei, K., Baglaenko, Y., Brenner, M., Loh, P., & Raychaudhuri, S. (2019). Fast, sensitive and accurate integration of single-cell data with Harmony. *Nature Methods*, *16*(12), 1289–1296. https://doi.org/10.1038/s41592-019-0619-0

Lause, J., Berens, P., & Kobak, D. (2021). Analytic Pearson residuals for normalization of single-cell RNA-seq UMI data. *Genome Biology*, *22*(1), 258. https://doi.org/10.1186/s13059-021-02451-7

Lavdovskaia, E., Denks, K., Nadler, F., Steube, E., Linden, A., Urlaub, H., Rodnina, M. V., & Richter-Dennerlein, R. (2020). Dual function of GTPBP6 in biogenesis and recycling of human mitochondrial ribosomes. *Nucleic Acids Research*, *48*(22), 12929–12942. https://doi.org/10.1093/nar/gkaa1132

Lee, B. B., & Sun, H. (2009). The chromatic input to cells of the magnocellular pathway of primates. *Journal of Vision*, *9*(2), 15. https://doi.org/10.1167/9.2.15

Lein, E., Borm, L. E., & Linnarsson, S. (2017). The promise of spatial transcriptomics for neuroscience in the era of molecular cell typing. *Science*, *358*(6359), 64–69. https://doi.org/10.1126/science.aan6827

Lerma, J., Morales, M., Vicente, M. A., & Herreras, O. (1997). Glutamate receptors of the kainate type and synaptic transmission. *Trends in Neurosciences*, *20*(1), 9–12. https://doi.org/10.1016/S0166-2236(96)20055-4

Levitt, J. B., Schumer, R. A., Sherman, S. M., Spear, P. D., & Movshon, J. A. (2001). Visual response properties of neurons in the LGN of normally reared and visually deprived macaque monkeys. *Journal of Neurophysiology*, *85*(5), 2111–2129. https://doi.org/10.1152/jn.2001.85.5.2111

816 Lowe, R., Shirley, N., Bleackley, M., Dolan, S., & Shafee, T. (2017). Transcriptomics
817 technologies. *PLOS Computational Biology*, *13*(5), e1005457.
818 https://doi.org/10.1371/journal.pcbi.1005457
819 Maunsell, J. H. R., Ghose, G. M., Assad, J. A., McADAMS, C. J., Boudreau, C. E., & Noerager,
820 B. D. (1999). Visual response latencies of magnocellular and parvocellular LGN neurons
821 in macaque monkeys. *Visual Neuroscience*, *16*(1), 1–14.
822 https://doi.org/10.1017/S0952523899156177
823 McInnes, L., Healy, J., & Melville, J. (2020). UMAP: Uniform Manifold Approximation and
824 Projection for Dimension Reduction. *arXiv:1802.03426 [Cs, Stat]*.
825 http://arxiv.org/abs/1802.03426
826 Müller, T., Braud, S., Jüttner, R., Voigt, B. C., Paulick, K., Sheean, M. E., Klisch, C.,
827 Gueneykaya, D., Rathjen, F. G., Geiger, J. R., Poulet, J. F., & Birchmeier, C. (2018).
828 Neuregulin 3 promotes excitatory synapse formation on hippocampal interneurons. *The*
829 *EMBO Journal*, *37*(17), e98858. https://doi.org/10.15252/embj.201798858
830 Noseda, R., Borsook, D., & Burstein, R. (2017). Neuropeptides and Neurotransmitters That
831 Modulate Thalamo-Cortical Pathways Relevant to Migraine Headache. *Headache*, *57*
832 *Suppl 2*(Suppl 2), 97–111. https://doi.org/10.1111/head.13083
833 Peng, Y.-R., Shekhar, K., Yan, W., Herrmann, D., Sappington, A., Bryman, G. S., Zyl, T. van,
834 Do, M. T. H., Regev, A., & Sanes, J. R. (2019). Molecular Classification and
835 Comparative Taxonomics of Foveal and Peripheral Cells in Primate Retina. *Cell*, *176*(5),
836 1222-1237.e22. https://doi.org/10.1016/j.cell.2019.01.004
837 Pietersen, A. N. J., Cheong, S. K., Solomon, S. G., Tailby, C., & Martin, P. R. (2014). Temporal
838 response properties of koniocellular (blue-on and blue-off) cells in marmoset lateral

839 geniculate nucleus. *Journal of Neurophysiology*, *112*(6), 1421–1438.
840 https://doi.org/10.1152/jn.00077.2014
841 Reid, R. C., & Shapley, R. M. (2002). Space and Time Maps of Cone Photoreceptor Signals in
842 Macaque Lateral Geniculate Nucleus. *Journal of Neuroscience*, *22*(14), 6158–6175.
843 https://doi.org/10.1523/JNEUROSCI.22-14-06158.2002
844 Rousso, D. L., Qiao, M., Kagan, R. D., Yamagata, M., Palmiter, R. D., & Sanes, J. R. (2016).
845 Two Pairs of ON and OFF Retinal Ganglion Cells Are Defined by Intersectional Patterns
846 of Transcription Factor Expression. *Cell Reports*, *15*(9), 1930–1944.
847 https://doi.org/10.1016/j.celrep.2016.04.069
848 Schneider, I., Cepela, J., Shetty, M., Wang, J., Nelson, A. C., Winterhoff, B., & Starr, T. K.
849 (2021). Use of "default" parameter settings when analyzing single cell RNA sequencing
850 data using Seurat: A biologist's perspective. *Journal of Translational Genetics and*
851 *Genomics*, *5*(1), 37–49. https://doi.org/10.20517/jtgg.2020.48
852 Schneider, K. A., Richter, M. C., & Kastner, S. (2004). Retinotopic Organization and Functional
853 Subdivisions of the Human Lateral Geniculate Nucleus: A High-Resolution Functional
854 Magnetic Resonance Imaging Study. *Journal of Neuroscience*, *24*(41), 8975–8985.
855 https://doi.org/10.1523/JNEUROSCI.2413-04.2004
856 Sherman, S. M., & Guillery, R. W. (2006). *Exploring the thalamus and its role in cortical*
857 *function, 2nd ed* (pp. xxi, 484). MIT Press.
858 Shibata, R., Nakahira, K., Shibasaki, K., Wakazono, Y., Imoto, K., & Ikenaka, K. (2000). A-
859 Type K+ Current Mediated by the Kv4 Channel Regulates the Generation of Action
860 Potential in Developing Cerebellar Granule Cells. *Journal of Neuroscience*, *20*(11),
861 4145–4155. https://doi.org/10.1523/JNEUROSCI.20-11-04145.2000

862 Sincich, L. C., Park, K. F., Wohlgemuth, M. J., & Horton, J. C. (2004). Bypassing V1: A direct
863 geniculate input to area MT. *Nature Neuroscience*, *7*(10), 1123–1128.
864 https://doi.org/10.1038/nn1318
865 Solomon, S. G., & Lennie, P. (2007). The machinery of colour vision. *Nature Reviews.*
866 *Neuroscience*, *8*(4), 276–286. https://doi.org/10.1038/nrn2094
867 Solomon, S. G., Tailby, C., Cheong, S. K., & Camp, A. J. (2010). Linear and Nonlinear
868 Contributions to the Visual Sensitivity of Neurons in Primate Lateral Geniculate Nucleus.
869 *Journal of Neurophysiology*. https://doi.org/10.1152/jn.01118.2009
870 Solomon, S. G., White, A. J. R., & Martin, P. R. (2002). Extraclassical Receptive Field
871 Properties of Parvocellular, Magnocellular, and Koniocellular Cells in the Primate Lateral
872 Geniculate Nucleus. *Journal of Neuroscience*, *22*(1), 338–349.
873 https://doi.org/10.1523/JNEUROSCI.22-01-00338.2002
874 St. Laurent, G., Shtokalo, D., Tackett, M. R., Yang, Z., Vyatkin, Y., Milos, P. M., Seilheimer, B.,
875 McCaffrey, T. A., & Kapranov, P. (2013). On the importance of small changes in RNA
876 expression. *Methods*, *63*(1), 18–24. https://doi.org/10.1016/j.ymeth.2013.03.027
877 Ståhl, P. L., Salmén, F., Vickovic, S., Lundmark, A., Navarro, J. F., Magnusson, J., Giacomello,
878 S., Asp, M., Westholm, J. O., Huss, M., Mollbrink, A., Linnarsson, S., Codeluppi, S.,
879 Borg, Å., Pontén, F., Costea, P. I., Sahlén, P., Mulder, J., Bergmann, O., … Frisén, J.
880 (2016). Visualization and analysis of gene expression in tissue sections by spatial
881 transcriptomics. *Science*, *353*(6294), 78–82. https://doi.org/10.1126/science.aaf2403
882 Stuart, T., Butler, A., Hoffman, P., Hafemeister, C., Papalexi, E., Mauck, W. M., Hao, Y.,
883 Stoeckius, M., Smibert, P., & Satija, R. (2019). Comprehensive integration of single-cell
884 data. *Cell*, *177*(7), 1888-1902.e21. https://doi.org/10.1016/j.cell.2019.05.031

885 Sugiyama, H., Ito, I., & Hirono, C. (1987). A new type of glutamate receptor linked to inositol
886 phospholipid metabolism. *Nature*, *325*(6104), 531–533. https://doi.org/10.1038/325531a0
887 Sun, S. H., Killian, N. J., & Pezaris, J. S. (2024). *More than expected: Extracellular waveforms*
888 *and functional responses in monkey LGN* (p. 2023.11.22.568065). bioRxiv.
889 https://doi.org/10.1101/2023.11.22.568065
890 Szíber, Z., Drouet, A., Mondin, M., Levet, F., & Thoumine, O. (2024). Neuroligin-1 dependent
891 phosphotyrosine signaling in excitatory synapse differentiation. *Frontiers in Molecular*
892 *Neuroscience*, *17*, 1359067. https://doi.org/10.3389/fnmol.2024.1359067
893 Tailby, C., Solomon, S. G., & Lennie, P. (2008). Functional Asymmetries in Visual Pathways
894 Carrying S-Cone Signals in Macaque. *Journal of Neuroscience*, *28*(15), 4078–4087.
895 https://doi.org/10.1523/JNEUROSCI.5338-07.2008
896 Tasic, B., Yao, Z., Graybuck, L. T., Smith, K. A., Nguyen, T. N., Bertagnolli, D., Goldy, J.,
897 Garren, E., Economo, M. N., Viswanathan, S., Penn, O., Bakken, T., Menon, V., Miller,
898 J., Fong, O., Hirokawa, K. E., Lathia, K., Rimorin, C., Tieu, M., … Zeng, H. (2018).
899 Shared and distinct transcriptomic cell types across neocortical areas. *Nature*, *563*(7729),
900 Article 7729. https://doi.org/10.1038/s41586-018-0654-5
901 Toth, M. E., Gonda, S., Vigh, L., & Santha, M. (2010). Neuroprotective effect of small heat
902 shock protein, Hsp27, after acute and chronic alcohol administration. *Cell Stress &*
903 *Chaperones*, *15*(6), 807–817. https://doi.org/10.1007/s12192-010-0188-8
904 Tripathy, R., Leca, I., Dijk, T. van, Weiss, J., Bon, B. W. van, Sergaki, M. C., Gstrein, T.,
905 Breuss, M., Tian, G., Bahi-Buisson, N., Paciorkowski, A. R., Pagnamenta, A. T.,
906 Wenninger-Weinzierl, A., Martinez-Reza, M. F., Landler, L., Lise, S., Taylor, J. C.,
907 Terrone, G., Vitiello, G., … Keays, D. A. (2018). Mutations in MAST1 Cause Mega-

908 Corpus-Callosum Syndrome with Cerebellar Hypoplasia and Cortical Malformations.
909 *Neuron*, *100*(6), 1354-1368.e5. https://doi.org/10.1016/j.neuron.2018.10.044
910 Vries, S. E. J. de, Lecoq, J. A., Buice, M. A., Groblewski, P. A., Ocker, G. K., Oliver, M., Feng,
911 D., Cain, N., Ledochowitsch, P., Millman, D., Roll, K., Garrett, M., Keenan, T., Kuan,
912 L., Mihalas, S., Olsen, S., Thompson, C., Wakeman, W., Waters, J., … Koch, C. (2020).
913 A large-scale standardized physiological survey reveals functional organization of the
914 mouse visual cortex. *Nature Neuroscience*, *23*(1), 138–151.
915 https://doi.org/10.1038/s41593-019-0550-9
916 Wang, J., Agarwal, D., Huang, M., Hu, G., Zhou, Z., Ye, C., & Zhang, N. R. (2019). Data
917 denoising with transfer learning in single-cell transcriptomics. *Nature Methods*, *16*(9),
918 875–878. https://doi.org/10.1038/s41592-019-0537-1
919 Wang, J., Lu, T., Gui, Y., Zhang, X., Cao, X., Li, Y., Li, C., Liu, L., & Ding, Z. (2023).
920 HSPA12A controls cerebral lactate homeostasis to maintain hippocampal neurogenesis
921 and mood stabilization. *Translational Psychiatry*, *13*(1), 280.
922 https://doi.org/10.1038/s41398-023-02573-5
923 Webster, C. M., Tworig, J., Caval-Holme, F., Morgans, C. W., & Feller, M. B. (2020). The
924 Impact of Steroid Activation of TRPM3 on Spontaneous Activity in the Developing
925 Retina. *eNeuro*, *7*(2). https://doi.org/10.1523/ENEURO.0175-19.2020
926 Wei, J.-R., Hao, Z.-Z., Xu, C., Huang, M., Tang, L., Xu, N., Liu, R., Shen, Y., Teichmann, S. A.,
927 Miao, Z., & Liu, S. (2022). Identification of visual cortex cell types and species
928 differences using single-cell RNA sequencing. *Nature Communications*, *13*(1), 6902.
929 https://doi.org/10.1038/s41467-022-34590-1

930 Weston, C. R., & Davis, R. J. (2007). The JNK signal transduction pathway. *Current Opinion in*
931 *Cell Biology*, *19*(2), 142–149. https://doi.org/10.1016/j.ceb.2007.02.001
932 White, A. J. R., Solomon, S. G., & Martin, P. R. (2001). Spatial properties of koniocellular cells
933 in the lateral geniculate nucleus of the marmoset Callithrix jacchus. *The Journal of*
934 *Physiology*, *533*(2), 519–535. https://doi.org/10.1111/j.1469-7793.2001.0519a.x
935 Wiesel, T. N., & Hubel, D. H. (1966). Spatial and chromatic interactions in the lateral geniculate
936 body of the rhesus monkey. *Journal of Neurophysiology*, *29*(6), 1115–1156.
937 https://doi.org/10.1152/jn.1966.29.6.1115
938 Xu, X., Ichida, J. M., Allison, J. D., Boyd, J. D., Bonds, A. B., & Casagrande, V. A. (2001). A
939 comparison of koniocellular, magnocellular and parvocellular receptive field properties in
940 the lateral geniculate nucleus of the owl monkey (Aotus trivirgatus). *The Journal of*
941 *Physiology*, *531*(Pt 1), 203–218. https://doi.org/10.1111/j.1469-7793.2001.0203j.x
942 Yan, L., Herrington, J., Goldberg, E., Dulski, P. M., Bugianesi, R. M., Slaughter, R. S., Banerjee,
943 P., Brochu, R. M., Priest, B. T., Kaczorowski, G. J., Rudy, B., & Garcia, M. L. (2005).
944 Stichodactyla helianthus peptide, a pharmacological tool for studying Kv3.2 channels.
945 *Molecular Pharmacology*, *67*(5), 1513–1521. https://doi.org/10.1124/mol.105.011064
946 Yang, Y.-C., Hu, C.-C., & Lai, Y.-C. (2015). Non-additive modulation of synaptic transmission
947 by serotonin, adenosine, and cholinergic modulators in the sensory thalamus. *Frontiers in*
948 *Cellular Neuroscience*, *9*. https://doi.org/10.3389/fncel.2015.00060
949 Zeidan, A., & Ziv, N. E. (2012). Neuroligin-1 Loss Is Associated with Reduced Tenacity of
950 Excitatory Synapses. *PLOS ONE*, *7*(7), e42314.
951 https://doi.org/10.1371/journal.pone.0042314

952 Zhang, L., & McBain, C. J. (1995). Potassium conductances underlying repolarization and after-
953 hyperpolarization in rat CA1 hippocampal interneurones. *The Journal of Physiology*,
954 *488*(3), 661–672. https://doi.org/10.1113/jphysiol.1995.sp020998
955 Zheng, G. X. Y., Terry, J. M., Belgrader, P., Ryvkin, P., Bent, Z. W., Wilson, R., Ziraldo, S. B.,
956 Wheeler, T. D., McDermott, G. P., Zhu, J., Gregory, M. T., Shuga, J., Montesclaros, L.,
957 Underwood, J. G., Masquelier, D. A., Nishimura, S. Y., Schnall-Levin, M., Wyatt, P. W.,
958 Hindson, C. M., … Bielas, J. H. (2017). Massively parallel digital transcriptional
959 profiling of single cells. *Nature Communications*, *8*(1), 14049.
960 https://doi.org/10.1038/ncomms14049
961